AMERICAN SOCIETY FOR MICROBIOLOGY | Molecular and Cellular Biology®

RESEARCH ARTICLE

Yeast Sphingolipid Phospholipase Gene *ISC1* Regulates the Spindle Checkpoint by a *CDC55*-Dependent Mechanism

Nabil Matmati,[a,b,e] Bachar H. Hassan,[a,b] Jihui Ren,[a,b] Ashraf A. Shamssedine,[a,b] Eunmi Jeong,[a,b] Baasil Shariff,[a,b] Justin Snider,[a,b] Steven V. Rødkær,[g] Guocai Chen,[c] Bidyut K. Mohanty,[d] W. Jim Zheng,[c] Lina M. Obeid,[a,b,f†] Martin Røssel-Larsen,[g] Nils J. Færgeman,[g] Yusuf A. Hannun[a,b,d]

[a]The Stony Brook University Cancer Center, Stony Brook University, Stony Brook, New York, USA
[b]Department of Medicine, Stony Brook University, Stony Brook, New York, USA
[c]School of Biomedical Informatics, University of Texas Health Science Center at Houston, Houston, Texas, USA
[d]Department of Biochemistry and Molecular Biology, Medical University of South Carolina, Charleston, South Carolina, USA
[e]Department of Neurology, Rochester Regional Health, Rochester, New York, USA
[f]Northport Veterans Affairs Medical Center, Northport, New York, USA
[g]Villum Center for Bioanalytical Sciences, Department of Biochemistry and Molecular Biology, University of Southern Denmark, Odense, Denmark

Nabil Matmati and Bachar H. Hassan contributed equally to this work. Order was determined by initiation of the project and seniority.

ABSTRACT Defects in the spindle assembly checkpoint (SAC) can lead to aneuploidy and cancer. Sphingolipids have important roles in many cellular functions, including cell cycle regulation and apoptosis. However, the specific mechanisms and functions of sphingolipids in cell cycle regulation have not been elucidated. Using analysis of concordance for synthetic lethality for the yeast sphingolipid phospholipase *ISC1*, we identified two groups of genes. The first comprises genes involved in chromosome segregation and stability (*CSM3*, *CTF4*, *YKE2*, *DCC1*, and *GIM4*) as synthetically lethal with *ISC1*. The second group, to which *ISC1* belongs, comprises genes involved in the spindle checkpoint (*BUB1*, *MAD1*, *BIM1*, and *KAR3*), and they all share the same synthetic lethality with the first group. We demonstrate that spindle checkpoint genes act upstream of Isc1, and their deletion phenocopies that of *ISC1*. Reciprocally, *ISC1* deletion mutants were sensitive to benomyl, indicating a SAC defect. Similar to *BUB1* deletion, *ISC1* deletion prevents spindle elongation in hydroxyurea-treated cells. Mechanistically, PP2A-Cdc55 ceramide-activated phosphatase was found to act downstream of Isc1, thus coupling the spindle checkpoint genes and Isc1 to *CDC55*-mediated nuclear functions.

KEYWORDS ceramide, hydroxyurea, *ISC1*, *CDC55*, *SWE1*, cell cycle, spindle checkpoint, phosphoproteomics, budding yeast

The survival of cells and organisms requires accurate chromosome segregation. Chromosomal loss or missegregation can lead to aneuploidy and cancer development (1, 2). The spindle assembly checkpoint detects defects in spindle structure or in the alignment of chromosomes on the spindle and delays anaphase onset until these defects are corrected. More subtle defects, such as the presence of a single kinetochore that is not attached to spindle microtubules, can also activate the checkpoint (3). When the mitotic spindle assembly is impaired by microtubule-depolymerizing agents, such as nocodazole or benomyl, spindle checkpoint mutants fail to delay their cell cycle progression and die quickly because of chromosome loss (4).

In recent years, ceramide, sphingosine 1-phosphate, sphingosine, and ceramide 1-phosphate have emerged as bioactive sphingolipids implicated in many important cellular functions, such us cell growth, inflammation, and response to stress stimuli (5–7). Sphingolipid metabolism is conserved, for the most part, from budding yeasts to

Citation Matmati N, Hassan BH, Ren J, Shamssedine AA, Jeong E, Shariff B, Snider J, Rødkær SV, Chen G, Mohanty BK, Zheng WJ, Obeid LM, Røssel-Larsen M, Færgeman NJ, Hannun YA. 2020. Yeast sphingolipid phospholipase gene *ISC1* regulates the spindle checkpoint by a *CDC55*-dependent mechanism. Mol Cell Biol 40:e00340-19. https://doi.org/10.1128/MCB.00340-19.

Address correspondence to Yusuf A. Hannun, yusuf.hannun@stonybrookmedicine.edu.

† Deceased.

Received 25 July 2019
Returned for modification 19 August 2019
Accepted 18 March 2020
Accepted manuscript posted online 23 March 2020
Published 28 May 2020

mammals (8), and ceramide has been implicated as a transducer for stress stimuli in mammalian systems and in yeast (9–11).

The yeast sphingolipid phospholipase ISC1 is the main enzyme involved in the catabolism of complex sphingolipids in *Saccharomyces cerevisiae*; it hydrolyzes inositol phosphoceramides and related yeast complex sphingolipids to generate bioactive ceramide molecules (12, 13). However, it is now increasingly appreciated that ceramides represent a family of structurally and metabolically related molecules that may be differentially regulated and may mediate distinct signals (14). As a result, it is becoming increasingly important to define the biological processes affected by specific mechanisms and pathways of ceramide generation.

We showed previously that when cells lacking *ISC1* are treated with hydroxyurea (HU), they acquire an additional G_2/M block, which follows the S phase block normally seen in wild-type (WT) cells upon HU treatment (15). This result raised several intriguing questions as to how a sphingolipid enzyme can be involved in cell cycle regulation, the pathways implicated, and the underlying mechanisms involved.

In an effort to address these questions, we initially adopted a data-driven bioinformatics approach (16) using available genetic interaction databases. Extensive work has been done to infer functions from genetic interaction networks (17–20). In an elaboration of these approaches, one study showed that defining shared synthetic lethal partners may serve as an indication of functional relevance that can be used to infer gene functions (21).

In this study, synthetic lethality analysis identified a set of genes (*CSM3*, *CTF4*, *YKE2*, *DCC1*, and *GIM4*) involved in chromatid cohesion and chromosome segregation (22, 23), being synthetic lethal partners of *ISC1*. The analysis also identified another set of genes involved in the spindle assembly checkpoint that share these synthetic lethal partners with *ISC1*. We herein provide biochemical and biological evidence that *ISC1* functions in the spindle assembly checkpoint. We used quantitative phosphoproteomics analysis to identify potential phosphotargets downstream of Isc1, and this analysis revealed several nuclear phosphoproteins involved in cell division, spindle assembly, and kinetochore-microtubule attachment. We implicate a Cdc55-dependent mechanism in these actions. To our knowledge, this is the first report implicating a sphingolipid enzyme and consequently ceramides in the regulation of the spindle assembly checkpoint. They also provide a mechanism connecting Bub1 and other checkpoint regulators to activation of *CDC55* phosphatase.

RESULTS

Defining functional partners of Isc1 using synthetic lethality and genetic interaction network analysis. To better understand the unexpected role of Isc1 in the response to HU and DNA damage, we resorted to synthetic lethality analysis. We examined published databases to find synthetic lethal partners of Isc1 in *S. cerevisiae*. We then searched for genes that share the maximum number of synthetic lethal partners with *ISC1*. This approach identified four genes (*MAD1*, *BUB1*, *BIM1*, and *KAR3*) sharing the highest number of synthetically lethal genes with *ISC1*. Importantly, they all share the same 5 synthetic lethal partners (*CSM3*, *YKE2*, *CTF4*, *GIM4*, and *DCC1*) (Fig. 1A). Interestingly, *CSM3*, *YKE2*, *CTF4*, *GIM4*, and *DCC1* are all involved in sister chromatid cohesion, chromosomal segregation, and maintenance of telomere length. In contrast, the set of genes, namely, *MAD1*, *BUB1*, *BIM1*, and *KAR3*, showing synthetic lethality similar to that of *ISC1*, are mostly involved in spindle checkpoint. *MAD1* encodes a coiled-coil protein that is involved in the spindle assembly checkpoint. *BUB1* encodes a protein kinase that forms a complex with Mad1 and Bub3, which is crucial in the checkpoint mechanism required to prevent cell cycle progression into anaphase in the presence of spindle damage. *BIM1* produces a microtubule-binding protein that together with Kar9 makes up the cortical microtubule capture site and delays the exit from mitosis when the spindle is oriented abnormally. The *KAR3* gene encodes the minus-end-directed microtubule motor that functions in mitosis and meiosis, and it localizes to the spindle pole body. This protein is required for nuclear fusion during

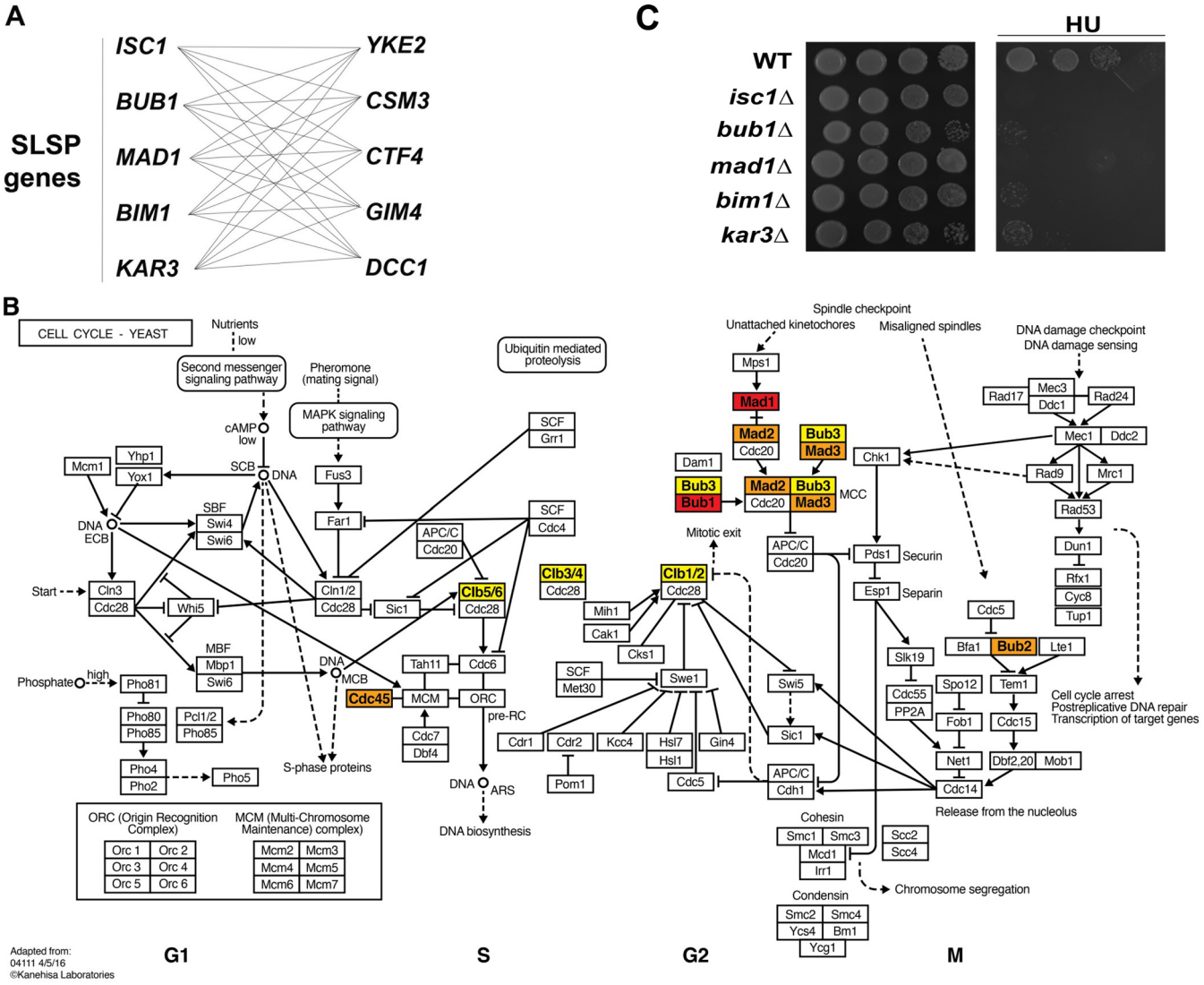

FIG 1 Identification of the SLSP genes through network analysis of synthetically lethality. (A) *ISC1* and its synthetically lethal partners. Genes on the left, SLSP genes, are the genes that share the highest number of synthetically lethal genes with *ISC1*, and the genes on the right are the synthetically lethal partners common with *ISC1*. (B) Cell cycle genes sharing at least one synthetic lethal partner with *ISC1*. Genes are colored by the number of synthetic lethal partners they share with *ISC1*: red, 5 shared partners; orange, 4 shared partners; yellow, 3, shared partners. Note that a majority of genes that share the maximum number of synthetic lethal partners with *ISC1* (in red) are clustered around the G_2/M phase, consistent with the experimental results showing that deletion of *ISC1* resulted in G_2/M arrest in HU-treated cells. Modified from original source, this panel originated from KEGG/GenomeNet (https://www.genome.jp/kegg/kegg1.html). (C) Elevated HU sensitivity of genes sharing synthetic lethal partners with *ISC1* (SLSP genes). The haploid wild-type (WT) strain was used, along with individual gene deletion mutants—*isc1*Δ, *bub1*Δ, *mad1*Δ, *bim1*Δ, and *kar3*Δ mutants—all derived from the WT strain. Spot testing was performed on YPD plates as described in Materials and Methods. This experiment was repeated three independent times, with similar results.

mating and is a potential Cdc28 substrate. Notably, the annotation of these genes indicates that most of them are related to cell cycle and chromosome segregation, consistent with the experimental data connecting *ISC1* to cell cycle regulation (15).

In addition to these four genes that share 5 synthetic lethal partners with *ISC1* (for ease of designation, we refer to this group of genes, on the left side of Fig. 1A, as *ISC1* synthetic lethal shared partner [SLSP] genes), we also identified 272 additional genes that share at least one of these synthetic lethal partners. Many of these genes are cell cycle genes, which can be mapped to the cell cycle pathway (Fig. 1B). Notably, genes sharing a majority of synthetic lethal partners with *ISC1* (colored in red and orange in Fig. 1B) all function at the G_2/M phase, consistent with the observation that deletion of *ISC1* resulted in the G_2/M arrest in HU-treated cells (15). These findings indicate that genetic interaction network is a powerful tool to dissect the function of the sphingolipid pathway in cell cycle progression and genome instability.

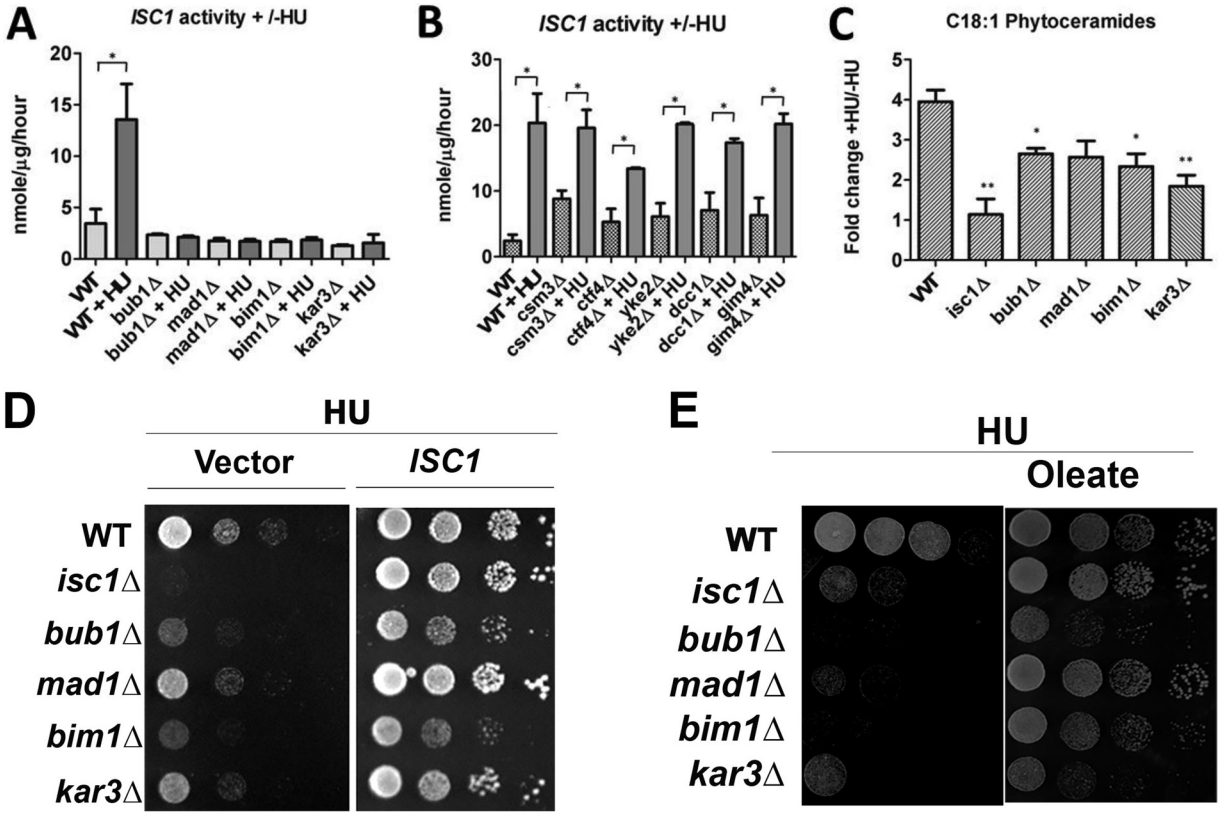

FIG 2 SLSP genes act upstream of *ISC1*. (A) Enzymatic activity of *ISC1*. Activity assays were performed on lysates of WT, *bub1*Δ, *mad1*Δ, *bim1*Δ, and *kar3*Δ cells in response to HU treatment. All cells were transformed with a vector containing *ISC1* under the control of the galactose promoter. For statistical analysis, the Student *t* test for paired sample means was used. *, $P \leq 0.05$. (B) Activity assay of *ISC1* and its synthetic lethal genes. The same activity assay was performed with the deletion mutants that are synthetically lethal with *isc1*Δ, *csm3*Δ, *ctf4*Δ, *yke*Δ, *dcc1*Δ, and *gim4*Δ mutants. The *ISC1* gene was overexpressed under the control of the galactose promoter in all strains as described for panel A. For statistical analysis, the Student *t* test for paired sample means was used. *, $P \leq 0.05$. (C) $C_{18:1}$ phytoceramide profile in *ISC1* and its SLSP genes. Levels of $C_{18:1}$ phytoceramides were determined using mass spectrometry in WT cells, *isc1*Δ cells, and cells of SLSP gene deletion mutants. The data show fold changes between untreated cells and cells treated with HU. The data represent the means from three independent experiments; the bars indicate standard errors of the means (SEM). For statistical analysis, the Student *t* test for paired sample means was used. *, $P \leq 0.05$; **, $P \leq 0.01$. (D) Effects of overexpression of *ISC1* on sensitivity of SLSP gene deletion strains to HU. A spot test was done to see if overexpression of *ISC1* is able to correct the SLSP gene sensitivity to HU. This experiment was repeated three independent times, with the same results. (E) Effects of oleate on sensitivity of SLSP gene deletion strains to HU. The WT, *isc1*Δ mutant, and all SLSP gene deletion mutant strains were spotted onto YPD plates containing 7.5 mg/ml of HU and 0.005% of oleate. This experiment was repeated three independent times, with similar results.

The synthetic lethality analysis suggested that the SLSP genes most likely participate in a common pathway with Isc1. Accordingly, we hypothesized that functional loss of these four genes should result in phenotypes resembling *isc1*Δ cells.

Since the *ISC1* deletion strain exhibits elevated HU sensitivity, we examined the ability of each of these four genes to phenocopy the deletion of *ISC1*. Figure 1C shows that deletion of any one of these four genes resulted in enhanced HU sensitivity.

Participation of Isc1 in a pathway regulated by SLSP genes. The above results suggested a close functional relationship between Isc1 and its partners. Since HU was shown to activate Isc1, we next sought to determine if Isc1 activity was regulated by Bub1, Mad1, Bim1, and Kar3, acting upstream of Isc1. The results showed that deletion of each of these genes abrogated the increase in Isc1 activity in response to HU (Fig. 2A). To determine if Isc1 activation by HU is influenced by the Csm3-related group (*CSM3*, *CTF4*, *YKE2*, *DCC1*, and *GIM4*), the activity of Isc1 was determined in deletion mutants of these genes in the presence and absence of HU. The results shown in Fig. 2B indicate that HU treatment activated Isc1 in each of these deletions. Taken together, these results demonstrate that activation of Isc1 depends on the function of Bub1, Mad1, Bim1, and Kar3 but not on its synthetic lethal partners and thus place Isc1 downstream of the SLSP group.

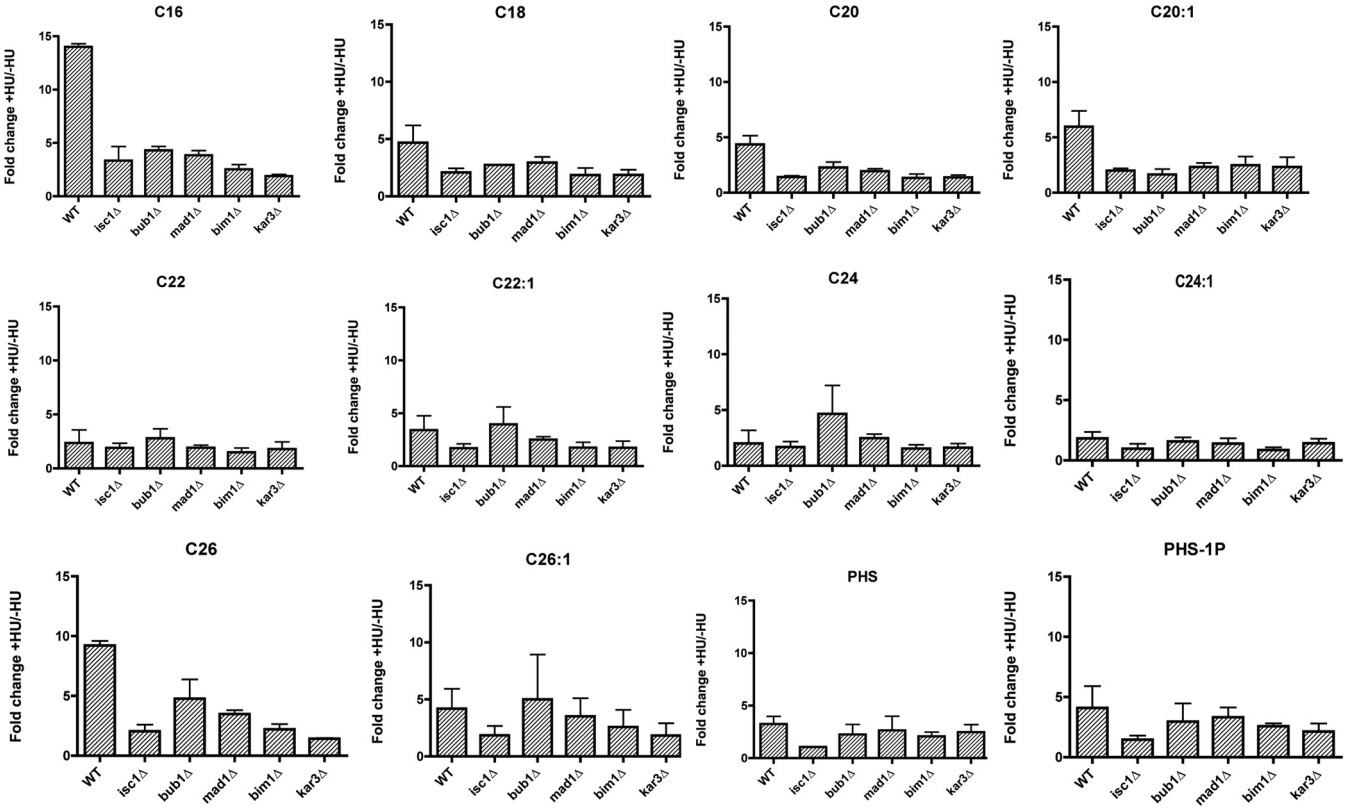

FIG 3 Phytoceramide level changes in the WT, *isc1*Δ mutant, and in all SLSP mutants upon HU treatment. Phytoceramide species changes are represented in each panel, showing the fold change of lipids following HU treatment for each chain length in the WT and in each of the *isc1*Δ, *bub1*Δ, *mad1*Δ, *bim1*Δ, and *kar3*Δ deletion mutants. The data represent the means from three independent experiments; the bars indicate SEM.

Curiously, deletion of each of *CSM3*, *CTF4*, *YKE2*, *DCC1*, and *GIM4* resulted in higher "basal" activity of Isc1. This may suggest that Isc1 participates in a checkpoint that is activated by problems in sister chromatid exchange and chromosome segregation.

To further support these results, we evaluated the sphingolipid response to HU. Phytoceramides, especially $C_{18:1}$ phytoceramide, have been shown to increase after treatment of WT cells with HU but fail to do so in *isc1*Δ cells (24). The phytoceramide profiles of *bub1*Δ, *mad1*Δ, *bim1*Δ, and *kar3*Δ cells following HU treatment were very similar to that of *isc1*Δ cells (Fig. 2C).

A third and functional approach to define whether Isc1 acts downstream of SLSP was to evaluate if Isc1 can rescue the phenotype of deletions of the SLSP group in response to HU. The results (Fig. 2D) show that Isc1 overexpression was indeed sufficient to protect *bub1*Δ, *mad1*Δ, *bim1*Δ, and *kar3*Δ cells from HU.

Finally, and based on our previous study showing that oleate ($C_{18:1}$ fatty acid) was the predominant fatty acid capable of protecting *isc1*Δ cells from HU toxicity because of its incorporation into $C_{18:1}$ phytoceramide (24), the effects of oleate on the growth of *bub1*Δ, *mad1*Δ, *bim1*Δ, and *kar3*Δ cells in response to HU were evaluated. The results showed that addition of oleate protected, at least partially, the mutants from HU toxicity (Fig. 2E). Taken together, these results demonstrate that Isc1 functions downstream of SLSP genes.

Noticeably, increase of other phytoceramide chain length species, such as C_{16}, C_{18}, C_{20}, $C_{20:1}$, $C_{22:1}$, $C_{24:1}$, C_{26}, $C_{26:1}$, sphingosine (SPH), and sphingosine-1-phosphate (SPH-1P), were found in WT cells following HU treatment, and these species failed to increase in *isc1*Δ cells. Similarly, *bub1*Δ, *mad1*Δ, *bim1*Δ, and *kar3*Δ cells had phytoceramide levels comparable to those in *isc1*Δ cells (Fig. 3).

Involvement of Isc1 in spindle checkpoint. The above results raised the possibility of a previously unappreciated role for Isc1 and its phytoceramide products in the

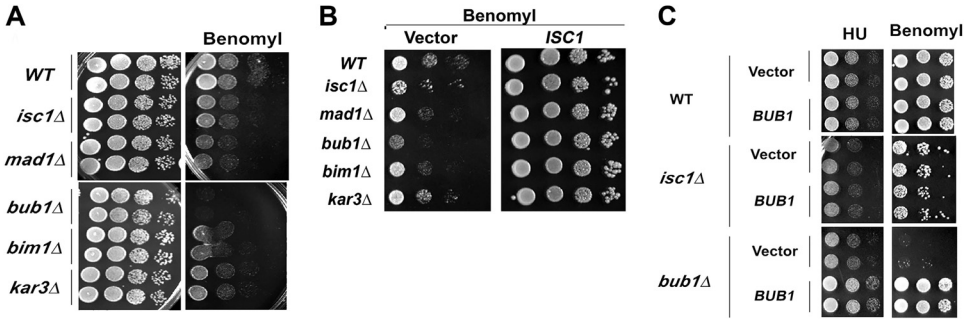

FIG 4 *ISC1* is involved in the spindle assembly checkpoint. (A) Sensitivity to benomyl. Spot tests were performed comparing growth on YPD plates containing 24 μg/ml of benomyl for WT, *isc1*Δ, and SLSP gene deletion strains. This experiment was performed three times, with the same results. (B) Overexpression of *ISC1* in benomyl-sensitive SLSP gene mutants. *ISC1* was overexpressed in the SLSP gene deletion mutants, and sensitivity to 12 μg/ml of benomyl was determined. The images of spot test plates were taken after 3 days of incubation at 30°C. (C) Overexpression of *BUB1* in the *isc1*Δ mutant. *BUB1* was cloned into a multicopy YEp24 vector (2μ vector), and spot tests were done on URA$^-$ plates with 7.5 mg/ml of HU or with 12 μg/ml of benomyl. This experiment was performed three independent times, with similar results. Results are expressed as means ± SD. For statistical analysis, the Student *t* test for paired sample means was used. *, $P \leq 0.05$; **, $P \leq 0.01$.

regulation of the spindle checkpoint. Since sensitivity to benomyl indicates dysregulation of the spindle checkpoint, we evaluated the sensitivity of *isc1*Δ cells to this reagent. The results in Fig. 4A show that *ISC1* deletion rendered cells more sensitive to benomyl; however, the sensitivity of *isc1*Δ cells was less severe than that of *bub1*Δ cells but similar to those of *mad1*Δ, *bim1*Δ, and *kar3*Δ cells. Functionally, the results showed that overexpression of *ISC1* protected from the severe growth defect of *bub1*Δ cells and the slow growth phenotype of *mad1*Δ, *bim1*Δ, and *kar3*Δ strains in response to benomyl (Fig. 4B). To rule out the possibility of Isc1 acting upstream of Bub1, *BUB1* was overexpressed in an *isc1*Δ strain, the results showed that overexpression of *BUB1* had no protective effect on the *isc1*Δ strains in its response to HU or benomyl (Fig. 4C). Taken together, these results provide further evidence that Isc1 acts downstream of the SLSP group and is indeed a key mediator of their functions.

The sensitivity to benomyl and the ability of Isc1 to overcome the defects of Bub1 and partners suggested a role for Isc1 in spindle elongation. When WT cells were treated with HU, spindles became elongated (Fig. 5A, top). However, spindles were not elongated in *isc1*Δ or *bub1*Δ cells (Fig. 5A, middle and bottom, respectively). Another indicator of a spindle checkpoint deficiency is sensitivity to nocodazole (25). A spot test assay showed that deletion of *ISC1* rendered cells more sensitive to nocodazole (data not shown). Checkpoint mutants tend to have a premature sister chromatid separation in the presence of nocodazole. We used a strain expressing a Tet-green fluorescent protein (GFP) fusion and containing tandem repeats of the *tet* operator inserted into the chromosomes in WT and *isc1*Δ cells. The results shown in Fig. 5B, left side, indicate that the *isc1*Δ strain had more sister chromatid separation than the WT at 3 and 6 h in the presence of nocodazole. Separation of sister chromatids was assayed as the percentage of cells with two separated fluorescent dots as seen in Fig. 5B, right side.

Additionally, we performed a budding assay to establish if the *isc1*Δ strain followed a WT budding pattern or spindle checkpoint mutant pattern. Checkpoint mutants tend to continue to bud in the presence of nocodazole, whereas WT cells tend to have fewer buds as they arrest. Our results indicated that *isc1*Δ cells had higher budding pattern than the WT, but they had fewer buds than the *mad1*Δ spindle checkpoint mutant (Fig. 5C). Clearly, this result indicates that a higher proportion of *isc1*Δ cells than of WT cells continued to bud. Overexpression of *ISC1* was able to reduce the budding patterns of *isc1*Δ, *bub1*Δ, *mad1*Δ, *bim1*Δ, and *kar3*Δ cells to WT levels. This experiment showed that overexpression of *ISC1* is sufficient to halt budding increase in SLSP mutants in the presence of nocodazole. This result is additional evidence of the downstream role of Isc1 in the SLSP gene pathway.

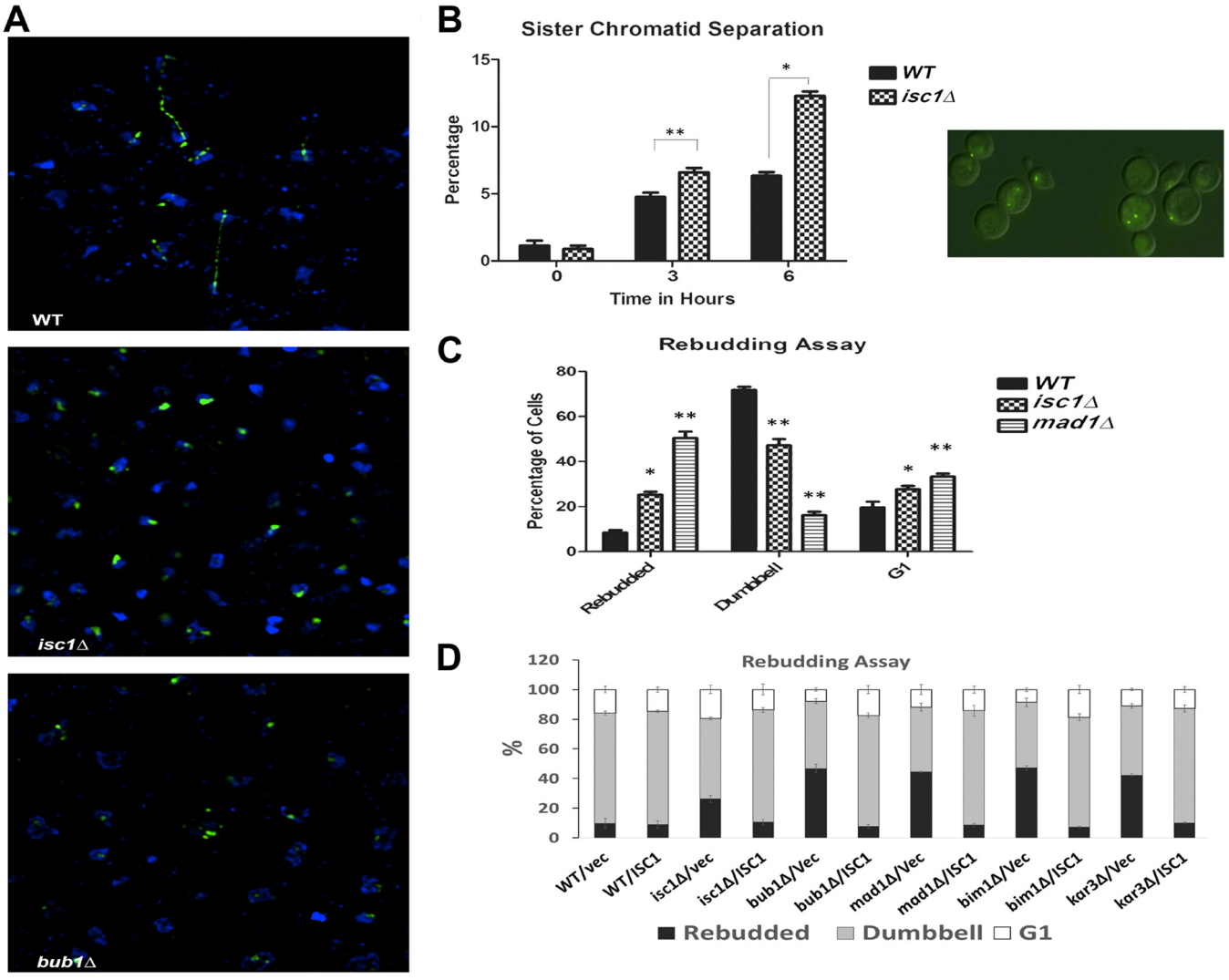

FIG 5 (A) Spindle elongation in WT and *isc1***Δ** cells and in *bub1*Δ cells in the presence of HU. Immunofluorescence was used to determine the elongation of tubulin using anti-alpha-tubulin antibody in WT, *isc1*Δ, and *bub1*Δ cells, all treated with HU. This experiment was performed three times, and all results were the same. (B) Sister chromatid separation assay was done in WT and *isc1*Δ cells in the presence of nocodazole at time zero and at 3 and 6 h. Experiments were performed three independent times. (C) Rebudding assay in WT, *isc1*Δ, and *mad1*Δ cells in the presence of nocodazole for 6 h. Rebudded cells, dumbbell cells, and cells in G_1 were quantified. (D) Overexpression of *ISC1* was done in WT, *isc1*Δ, *bub1*Δ, *mad1*Δ, *bim1*Δ, and *kar3*Δ cells to show if it can stop or decrease the budding. Experiments were performed three independent times. Results are expressed as means ± SD. For statistical analysis, the Student *t* test for paired sample means was used. *, $P \leq 0.05$; **, $P \leq 0.01$.

These phenotypes of *isc1*Δ cells, including defects in spindle elongation, sensitivity to nocodazole, and the increase in budding and sister chromatid separation in the presence of nocodazole, illustrate a previously unknown link between Isc1 and spindle elongation and sister chromatid separation. These results further corroborate the results on the very close functional roles of Isc1 and Bub1 (and its related partners).

Defining roles for Swe1 and Cdc55 downstream of Bub1 in spindle checkpoint. Previously, we found that deletion of Swe1 kinase rescued *isc1*Δ cells from HU sensitivity (15). This prompted us to investigate whether deletion of *SWE1* is able to protect *bub1*Δ, *mad1*Δ, *bim1*Δ, and *kar3*Δ cells from HU toxicity. The results showed that *SWE1* deletion indeed protected *bub1*Δ, *mad1*Δ, and *bim1*Δ cells from HU toxicity; however, it did not have a protective effect on *kar3*Δ cells from the action of HU (Fig. 6A). The results also showed that deletion of *SWE1* was able to correct the sensitivity of *bub1*Δ cells to benomyl (Fig. 6A), suggesting an interesting and previously unidentified role for Swe1 in protecting *bub1*Δ cells from benomyl toxicity. Deletion of *SWE1* also protected all the strains from the action of benomyl.

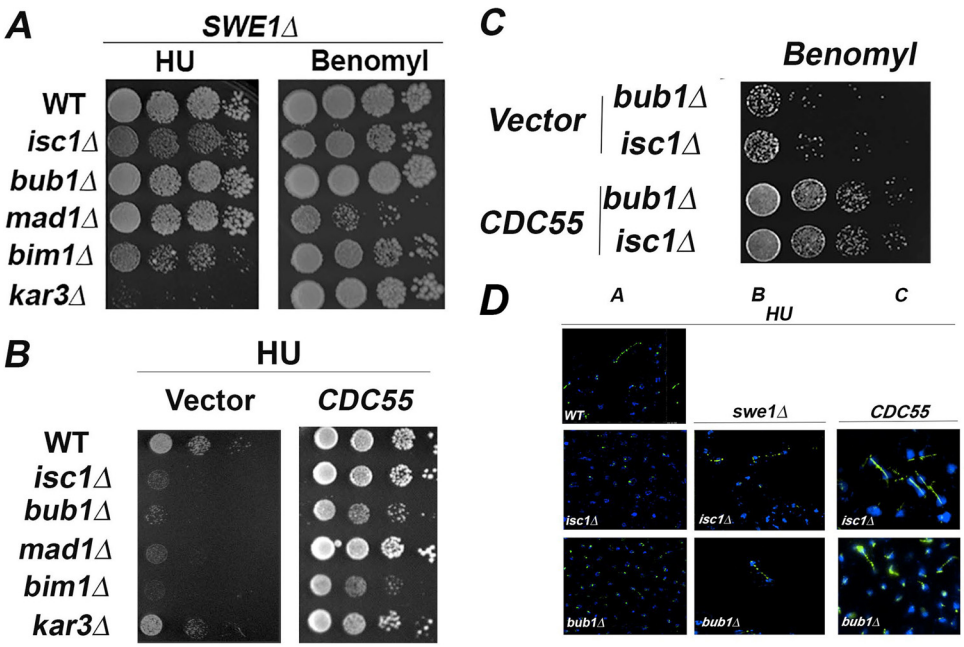

FIG 6 *SWE1* and *CDC55* are downstream targets for *ISC1*. (A) *SWE1* was deleted in *isc1*Δ cells and in all SLSP gene deletion mutants to assess sensitivity to HU and to benomyl. Cells were plated in YPD with or without 10 mg/ml of HU or 24 μg/ml of benomyl and incubated for 3 days at 30°C. (B) *CDC55* was overexpressed using a multicopy YEp24 vector and transformed in *isc1*Δ cells and in each of the SLSP mutant. The transformants were assed for HU sensitivity on plates containing HU or vehicle, and incubated for 3 days at 30°C. Images were taken at the end of incubation. (C) Overexpressed *CDC55* was assessed for its ability to protect *isc1*Δ and *bub1*Δ cells from benomyl toxicity. Spot tests were performed, and images were taken at the end of 3 days' incubation.These experiments were performed three independent times, and the results were the same. (D) Spindle elongation in WT, *isc1*Δ, and *bub1*Δ cells. Immunofluorescence was performed with single mutants to assess the elongation of spindles in the presence of HU. The spindle elongation in *isc1*Δ *swe*Δ and *bub1*Δ *swe1*Δ double mutants with HU is shown in panel B. Spindle elongation in *isc1*Δ cells and in *bub1*Δ cells overexpressing *CDC55* in the presence of HU is shown in panel C. Fixed cells were stained with anti-alpha-tubulin antibody and 4′,6-diamidino-2-phenylindole (DAPI). This experiment was performed three times, and similar results were obtained.

We had also shown that cells lacking *ISC1* are able to overcome the sensitivity to HU by overexpressing Cdc55, the regulatory subunit of phosphatase PP2A and a direct downstream target for ceramide, the lipid product of Isc1 action (26). Deletion of *BUB1* was rescued by the overexpression of *CDC55* in the presence of HU or benomyl (Fig. 6B and C). Overexpression of *CDC55* was also able to rescue the sensitivity of *mad1*Δ, *bim1*Δ, and *kar3*Δ cells to HU (Fig. 6B).

Considering these results, we explored if deletion of *SWE1* or overexpression of *CDC55* could correct the spindle elongation defect seen in *isc1*Δ and *bub1*Δ cells. To this end, we checked *isc1*Δ *swe1*Δ and *bub1*Δ *swe1*Δ double mutants for defects in spindle elongation in the presence of HU. The results in Fig. 6D show that the spindle elongation in the *isc1*Δ *swe1*Δ and *bub1*Δ *swe1*Δ mutants was very similar to that in WT cells. Similar results were obtained when the *CDC55* gene was overexpressed in *isc1*Δ and *bub1*Δ strains (Fig. 6D), indicating that *CDC55* is a key transducer of these effects downstream of both Bub1 and Isc1.

Identification of Isc1- and Cdc55-dependent dephosphorylations. To untangle how Isc1 and Cdc55 regulate signaling networks, we resorted to whole-cell phosphoproteomics analysis using iTRAQ labeling (isobaric tags for relative and absolute quantitation). Wild-type, *isc1*Δ, and *cdc55*Δ strains and *isc1*Δ cells overexpressing *CDC55* (*CDC55*-OE cells) were treated with HU as described in Materials and Methods. Based on the preceding results, we reasoned that HU treatment induces Isc1-dependent activation of Cdc55, resulting in significant protein dephosphorylation, and that dephosphorylation of specific signaling components would be attenuated in the *isc1*Δ and *cdc55*Δ strains. Therefore, we searched for the profile in which phosphopeptide levels were

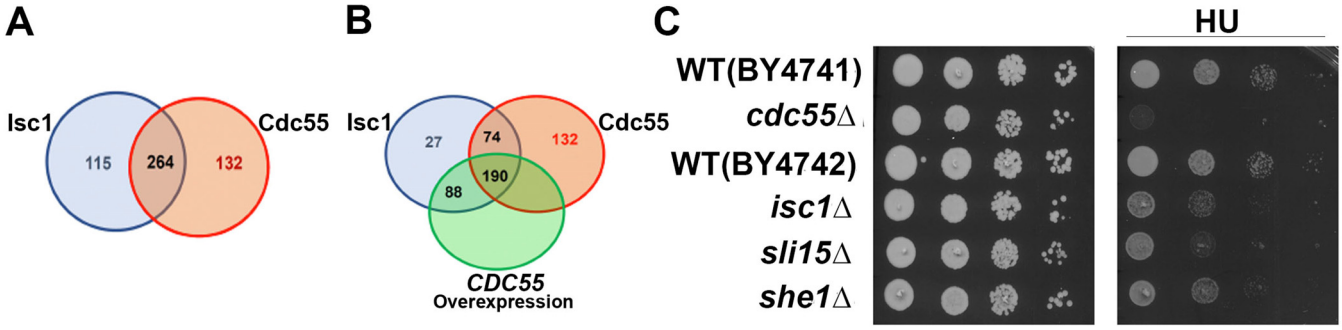

FIG 7 Potential substrates for PP2A-cdc55 phosphatase. (A) Venn diagrams showing the results of iTRAQ quantitative phosphoproteomics analysis. The diagram shows the overlapping of dephosphorylated proteins that are both Isc1 and Cdc55 dependent. A total of 264 proteins were found in the common group, while 115 proteins were unique to Isc1 and 132 proteins were unique to Cdc55. These results are strongly indicative that Cdc55 and Isc1 are in the same HU-induced pathway. (B) The diagram shows the overlapping of dephosphorylated peptides that are Isc1 and Cdc55 dependent and overcome by *CDC55* overexpression. Overexpression of *CDC55* was carried out in the *isc1*Δ mutant background. Of the 264 proteins common to Isc1 and Cdc55, 190 were reversed by *CDC55* overexpression while 74 proteins were not. Of the 115 proteins unique to the Isc1 group, 88 were reversed by *CDC55* overexpression while 27 were not. (C) Elevated HU sensitivity for the *sli15*Δ mutant strain. To test for HU sensitivity, haploid WT strains were used along with *cdc55*Δ, *isc1*Δ, *sli15*Δ, and *she1*Δ individual gene deletions, in the presence or absence of 10 mg/ml of HU and incubated for 2 days at 30°C. A volume of 3 μl was spotted onto YPD plates as follows: the first spot corresponds to and OD at 600 nm of ~0.3, and each subsequent spot is a 1:10 dilution of the preceding spot. The experiment was repeated three independent times, with similar results.

decreased in WT cells as a result of HU treatment (i.e., HU-induced dephosphorylation) but not in *isc1*Δ and *cdc55*Δ mutant cells (i.e., HU-induced dephosphorylation that is dependent on either Isc1 or Cdc55). Furthermore, to further implicate Cdc55 downstream of Isc1, we evaluated for phosphopeptide levels (whose decrease is lost in the *isc1*Δ cells) and that are then reversed by *CDC55* overexpression in the *isc1*Δ strain. This would establish Cdc55-dependent dephosphorylation. We identified 1,184 HU-induced dephosphorylations in WT cells, of which 545 phosphopeptides were Isc1 dependent, corresponding to 379 unique protein hits. We also identified 656 phosphopeptides that were Cdc55 dependent, corresponding to 396 unique protein hits, and 264 of these proteins (corresponding to 70% of the Isc1-dependent ones) were common to both Isc1 and Cdc55, strongly suggesting that Isc1 and Cdc55 are indeed in the same signaling pathway induced by HU. A Venn diagram is shown in Fig. 7A in which 264 proteins were common to Isc1 and Cdc55 while 115 and 132 proteins were unique to Isc1 and Cdc55, respectively. Importantly, out of the 545 Isc1-dependent phosphopeptides, 391 were overcome by *CDC55* overexpression, corresponding to 278 unique protein hits (Fig. 7B). Moreover, of the 264 proteins common to the Isc1 and Cdc55 groups, 190 protein phosphorylations (72%) were reversed by *CDC55* overexpression in the *isc1*Δ background strain. As a result, we have identified 190 proteins that were dephosphorylated in an Isc1- and Cdc55-dependent manner and whose phosphorylation levels were reversed by *CDC55* overexpression. These results strongly support the results from this study and previous ones (24, 26) that Cdc55 phosphatase is a key downstream mediator of ceramide actions in yeast and, in this case, especially in response to HU. While this study was in progress, Baro et al. reported a SILAC (stable-isotope labeling by amino acids in cell culture)-based phosphoproteomics study of a PP2A-Cdc55 mutant in which they identified 62 potential Cdc55 substrates (27). By comparing their results to our list of Isc1 and Cdc55-dependent phosphoproteins, we found a significant overlap of ~29%, strongly supporting the validity of our analysis.

Functional annotation of the 190 proteins. We then used David 6.7 to identify the biological processes mediated by Isc1 and Cdc55. The results obtained were sorted by fold enrichment (see Table S1 in the supplemental material). Functional annotation of the selected 190 proteins showed enrichment in several biological processes, including chromatin remodeling at centromeres, transmembrane trafficking, and cytoskeleton organization. In addition, there was a 5.5-fold enrichment in spindle microtubule gene ontology (GO) term and 3.6-fold enrichment in the mitotic cell cycle checkpoint proteins (Table S1). However, David and all other GO term software did not identify all

TABLE 1 Classification of the 190 genes obtained by phosphoproteomics analysis

Biological process	Genes	No.	%
Transport	*TAT1*, *PDR11*, *MNR2*, *HXT1*, *HXT3*, *YOR1*, *AVT4*, *RSB1*, *TRK1*, *ZRT3*, *HNM1*, *HXT7*, *YBT1*, *PDR5*, *ALR1*, *YPQ2*, *VTC2*, *ATM1*, *PHO84*, *SUL2*, *SAM3*, *AGP1*, *ALY2*, *HIP1*, *MUP1*, *CAN1*, *FPS1*, *ENA1*, *NHA1*, *VHT1*, *PHM7*	31	16.3
Spindle assembly and chromatid separation	*SHE1*, *SIZ1*, *NET1*, *TOP2*, *KCC4*, *ULP2*, *SLI15*, *SWE1*, *FIN1*, *DAM1*, *KIN4*, *GIP4*, *SPC29*, *SRC1*, *GAC1*, *STH1*	16	8.4
Vesicle trafficking	*SLY1*, *PTM1*, *YKT6*, *VPS53*, *SEC10*, *SEC16*, *EXO84*, *VTA1*, *EDE1*, *BSP1*, *ENT1*, *ENT2*, *SWA2*	13	6.8
Chromatin remodeling	*ISW1*, *SNF12*, *IES2*, *NGG1*, *STH1*, *RSC1*, *HST1*, *HOS3*, *SDS3*, *HOS4*, *CYC8*, *YNG2*	12	6.3
Metabolism	*PFK2*, *LEU1*, *YMR226C*, *GLK1*, *TCO89*, *PSK1*, *GPD2*, *CAT8*, *FAS2*	9	4.7
RNA processing	*EDC1*, *RPL25*, *TIF4632TCD89*, *JSN1*, *REF2*, *DCP2*, *SPT2*	8	4.2
Cytoskeleton organization	*SAC7*, *CRN1*, *ABP1*, *PIK1*, *NUM1*, *SPA2*	6	3.1
Protein phosphatase type 1 regulator activity	*GIP4*, *GAC1*, *REG1*, *SHP1*, *FIN1*	5	2.6
Polyamine metabolism	*HAA1*, *TPO3*, *TPO4*, *PTK2*	4	2.1
Budding	*ACE2*, *BEM2*, *IQG1*, *CDC3*	4	2.1
Cell cycle	*ORC2*, *RAD16*, *POL1*, *CDC37*	4	2.1
Translation initiation	*SUI3*, *SUI2*, *EAP1*, *TIF4632*	4	2.1
Splicing	*STP3*, *RRP15*, *EXO84*, *SPP2*	4	2.1

the spindle assembly proteins that were present in our list, as these genes were scattered among other categories. As a result, we sorted the 190 proteins manually, and the results are displayed in Table 1. We found 16 proteins (8.4%) that are related to spindle assembly and chromatid separation and thus were selected for further analysis. The proteins are She1, Siz1, Net1, Top2, Kcc4, Ulp2, Sli15, Swe1, Fin1, Dam1, Kin4, Gip4, Spc29, Src1, Gac1, and Sth1.

Isc1 and Cdc55 control the spindle checkpoint. Among the 16 proteins selected, some are known to be Cdc55 substrates, such as Swe1 and Net1. Particularly, Orc2, Kin4, Sli15 (INCEMP), Dam1, and She1 stood out since they are intimately associated with proper chromosome segregation and SAC regulation.

Orc2 is implicated in the initiation of DNA replication during S phase but is located on kinetochores during mitosis. In addition, Orc2 in yeast was implicated in sister chromatid cohesion, and its removal was found to induce SAC activation (28). Thus, Orc2 appears to function as a mediator of the actions of Isc1 and Cdc55 on the spindle checkpoint.

In yeast, Sli15-Ipl1-Bir1 form a complex called the chromosomal passenger complex (CPC) which associates with kinetochores in metaphase and with spindle midzone microtubules in anaphase. The CPC regulates key mitotic events: correction of chromosome microtubule attachment errors, activation of the spindle assembly checkpoint, and construction and regulation of the contractile apparatus that drives cytokinesis (29). As a result, the CPC is one of the main controllers of mitosis. Cdc14 dephosphorylates Sli15 and thereby directs the CPC to the spindle midzone and away from kinetochores, which contributes to mitotic exit. As a result, the CPC appears to be an important target for Cdc55 in this pathway. This could also explain the abundance of protein hits involved in budding and cytoskeleton organization that were obtained from phosphoproteomics analysis given the important role for CPC in cytokinesis (Table 1). Aurora-B/Ipl1 kinase detects and destabilizes incorrect sister chromatid attachments through control of kinesin MCAK, the DASH complex, and the Hec1 complex at the microtubule-kinetochore interface (30, 31). Dam1 is part of the DASH complex, as it couples the kinetochores to spindle microtubules. Dam1 is directly activated by Ipl1-mediated phosphorylation on S292 and is essential for proper chromosome segregation. Interestingly, the Dam1 dephosphorylation site in our phosphoproteomics data was found to be on the same S292 residue (the Ipl1 phosphorylation site). She1 is also a mitotic spindle protein that interacts with the Dam1 (DASH) complex, Sli15, and Bim1. In our phosphoproteomics data, the She1 dephosphorylation site was found to be on S165. Thus, Dam1 and its interacting partner She1 appear to be important targets for Isc1/Cdc55 in this HU-induced pathway.

TABLE 2 Summary of Isc1- and Cdc55-dependent dephosphorylations of selected proteins involved in the spindle assembly checkpoint found among the selected group of 190 proteins

Protein	Sequence[a]	Phosphorylation site	Function	Reference(s)
Swe1	*TNSPISLK	S133	Cdc28 kinase site	60, 61
Kcc4	*IAASLSDDDLKEDNDK	S894	Unknown	62–64
Net1	*AEGSKEPEK	S892	Unknown	65
	*VRPSLSSLSDLVSR	S1082	*cdk1* site	
	*SFISAK	S1161	Unknown	
Sli15	*TGSRPHSISPTK	S421		66
		S425		
		S427	Inhibit targeting the chromosomal passenger complex to spindle during preanaphase and inhibit SAC reactivation during anaphase	
Dam1	*NSIASGADLPIENDNVVNLGDLHPNNRISLGSGAAR	S292	Ipl1 (Aurora B kinase) phosphorylation site	65, 67–69
She1	*LRNSLVNGNDIVAR	S165	*cdk1* site	65
Kin4	*TSCGSPCYAAPELVVSTK	T209	ELM1 (kinase)	70

[a]The detected phosphorylation sites are underlined.

Kin4 is a serine/threonine protein kinase which inhibits the mitotic exit network (MEN). It is activated by Elm1 kinase and prevents cell cycle progression when the spindle position checkpoint (SPOC) is activated. From our phosphoproteomics data, Cdc55 appears to dephosphorylate Kin4 on its T209 residue (the same Elm1 kinase phosphorylation site). As a result, Kin4 and the SPOC appear to be targeted by Cdc55 and Isc1 in this pathway. More importantly, Sli15 (INCEMP) is hyperphosphorylated on S421, S425, and S427 in an Isc1- and Cdc55-dependent manner (Table 2). To determine whether Sli15 or any of the selected proteins are involved in this signaling pathway, we tested the sensitivity of several knockout mutants to hydroxyurea and compared it to those of *cdc55*Δ and *isc1*Δ mutants (Fig. 7C). The results indicate that the *sli15*Δ mutant is sensitive to hydroxyurea treatment and that its sensitivity is comparable to that of the *isc1*Δ mutant. On the other hand, a *she1*Δ knockout mutant showed no significant hydroxyurea sensitivity (Fig. 7C). This result corroborates the phosphoproteomics data and indicates that Sli15 is involved in this pathway downstream of Isc1 and Cdc55.

At the metaphase-anaphase transition, APC/cdc20 polyubiquitinates securin and causes separase activation. In turn, separase promotes sister chromatid separation by cleaving the cohesion complex. Separase can also regulate INCENP (Sli15)-Aurora B (Ipl1) anaphase spindle function through Cdc14 released from Net1 entrapment in the nucleolus (Fig. 8).

DISCUSSION

Overall, these new findings define a novel and unexpected role of an enzyme of sphingolipid metabolism, *ISC1*, in the spindle checkpoint. Specifically, the results strongly assign the action of *ISC1* to the function of *BUB1*, *MAD1*, *BIM1*, and *KAR3*. The identification of this group of genes was the result of an informatic approach aimed at matching the largest group of *ISC1*'s synthetically lethal partners (*YKE2*, *CSM3*, *CTF4*, *GIM4*, and *DCC1*) to genes that, like *ISC1*, are synthetically lethal to the same gene group. Both groups of genes are involved in chromatid separation and checkpoint operation. The first group is intimately involved in chromatin remodeling, chromosome segregation, and sister chromatid cohesion (22, 32). In contrast to this "mechanical'" function, the second group (the SLSP group) is involved in the G_2/M transition and the spindle checkpoints (25, 33).

Interestingly, these results offer a rather unappreciated explanation of synthetic lethality. Classically, synthetic lethality has been assumed to indicate the operation of two redundant pathways. The current results demonstrate that the two arms (Fig. 1A) have distinct functions. Defects in the chromatid separation machinery (right-side genes in Fig. 1A) are not lethal as long as the checkpoint machinery is intact. Likewise, defects in the checkpoint machinery would not be expected to be lethal unless

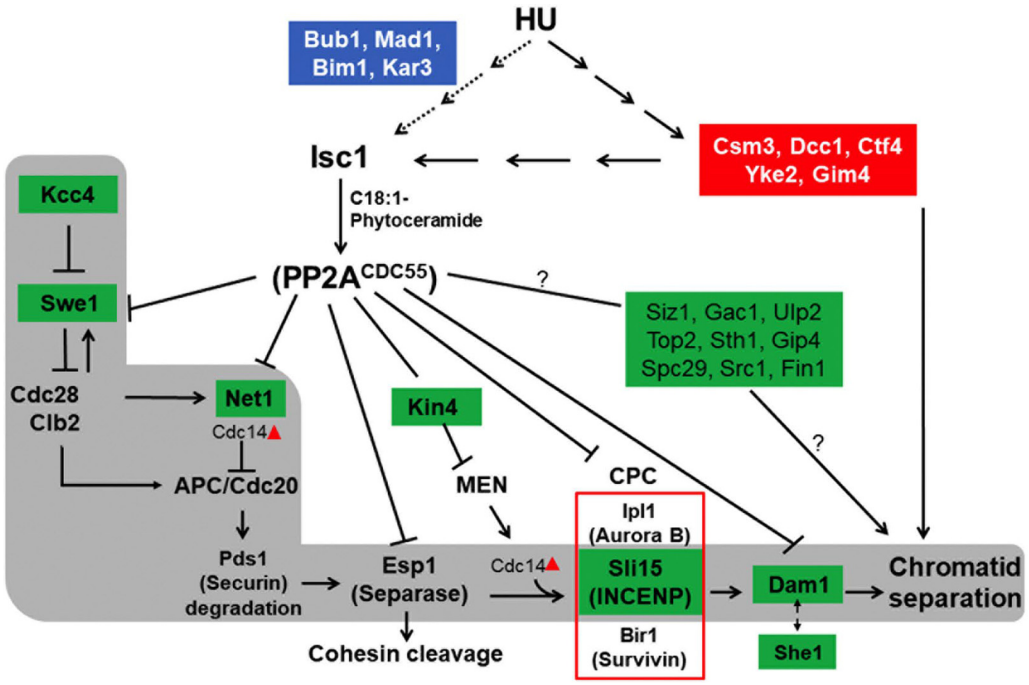

FIG 8 Proposed model for the role of Isc1 and Cdc55 in the HU-induced signaling pathway. When cells are treated with HU, a checkpoint signal would be activated through the SLPS genes. SLPS genes transmit the signal to Isc1, which produces $C_{18:1}$ phytoceramides, which functions as a signal to directly activate Cdc55 and thus its downstream targets Cdc16, Cdc23, Cdc27, Cdc14, Net1, Clb2, and Clb5 or inhibit *SWE1* kinase and its target Cdc28 kinase. Cdc55 phosphatase activity controls Cdc28 and APC/cdc20 activity through its multiple downstream targets. Swe1 can act directly on the activation of Cdc28, which then acts on APC/cdc20, with the latter triggering chromatid separation through pds1 (securin), Esp1 (separase), and cohesin cleavage. Separase can also regulate INCENP (Sli15)-Aurora B (Ipl1) anaphase spindle function through Cdc14 released from Net1 entrapment in the nucleolus. Cdc14 dephosphorylates Sli15 and thereby directs the chromosomal passenger complex (CPC) to the spindle midzone and away from kinetochores. Dam1, part of the DASH complex, couples the kinetochores to spindle microtubules. Dam1 is directly activated by Ipl1 phosphorylation and is essential for proper chromosome segregation. Dam1 interacts with another mitotic spindle protein, She1. Kin4 is activated by Elm1 kinase, it inhibits the mitotic exit network (MEN), and it prevents cell cycle progression when the spindle position checkpoint (SPOC) is activated. SLSP proteins are highlighted in blue, Csm3-related proteins in red. Potential Cdc55 substrates, identified in our phosphoproteomics study, are highlighted in green.

challenged by complications in sister chromatid separation. Thus, synthetic lethality is generated when there is a combination of a defect in the machinery along with a defect in the checkpoint.

From a "guilt by association" standpoint, these results suggested a specific role for *ISC1* in the physiology of chromosome separation, and by belonging to the SLSP group, more specifically in the checkpoints involved.

Our previous studies clearly suggested the involvement of Isc1 in the response to HU; however, it was not clear how Isc1 fits in the overall DNA damage response and checkpoint operations (15, 24). The results from this study resolve that issue and further identify Isc1 partners that act upstream of Isc1 and downstream of it in the genotoxic effects of HU.

Our approach assigned *ISC1* to the SLSP group of genes, suggesting they belong to the same pathway in the response to chromatid separation defects and spindle point activation. Experimentally, the results showed that deletion of *BUB1*, *MAD1*, *BIM1*, and *KAR3* phenocopies the deletion of *ISC1* in their sensitivity to HU. In addition, our data showed that deletion of *ISC1* gene yielded a phenotype similar to that yielded by the deletion of *MAD1*, known to play a role in spindle checkpoint and a member of the SLSP group of genes. In fact, *isc1*Δ cells, like *mad1*Δ cells, were more sensitive to nocodazole, had more budded cells, and showed a higher percentage of sister chromatid separation than the WT in the presence of nocodazole. Mechanistically, deletion of SLSP genes obliterated the increase in Isc1 activity in response to HU treatment and also abrogated

the increase in $C_{18:1}$ phytoceramides down to levels shown in the absence of treatment. Other chain length phytoceramides (C_{14}, $C_{14:1}$, C_{16}, $C_{16:1}$, C_{18}, C_{20}, $C_{20:1}$, C_{22}, $C_{22:1}$, C_{24}, $C_{24:1}$, C_{26}, and $C_{26:1}$) also increased following HU treatment. Among all chain length species, it was shown that $C_{18:1}$ phytoceramides were the most likely lipid mediator to protect cells from HU toxicity (24). Taken together, these results indicate that *ISC1* is regulated downstream of the SLSP genes. This was further corroborated by demonstrating that overexpression of the *ISC1* gene in the SLSP deletion mutants corrected their HU sensitivity phenotype. *ISC1* overexpression also corrected the sensitivity to benomyl of the SLSP gene deletion, further cementing this connection downstream of the SLSP genes (Fig. 8). Although the *isc1*Δ mutant did not show strong sensitivity to benomyl, additional experiments indicated that the *isc1*Δ mutant had a spindle elongation defect similar to that of the *bub1*Δ mutant when treated with HU. In the chromatid separation assay, we also found that the *isc1*Δ mutant had earlier chromatid separation than did the WT in the presence of nocodazole. This experiment provided further evidence implicating *ISC1* in the spindle checkpoint. In addition, an *isc1*Δ rebudding assay showed a higher percentage of budding cells than for the WT when treated with nocodazole. This assay showed the *isc1*Δ mutant to follow a spindle checkpoint mutant pattern of budding, although not as highly as the *mad1*Δ mutant. *ISC1* overexpression was able to correct the growth defect in all SLSP mutants. Furthermore, deletion of the *SWE1* gene did rescue growth on benomyl similarly in *isc1*Δ and SLSP mutants. Like in the *isc1*Δ mutant, overexpression of *CDC55* rescued growth on benomyl in *bub1*Δ. These data strongly link *ISC1* to the SLSP genes.

Importantly, this intimate connection of *ISC1* to the SLSP genes suggested that *ISC1* participates in key regulatory events mediated by Bub1 and Mad1. Indeed, Bub1 has important roles in the spindle checkpoint whereby it responds to many physical or mechanical events that occur in response to upstream alterations in chromosome separation (34). Bub1 and Mad1 are both members of the spindle assembly checkpoint, consisting of three functional units: a sensor, a signal transducer, and an effector. Importantly, while spindle elongation was detected in WT cells treated with HU, indicating that elongation mechanism was intact, *isc1*Δ and *bub1*Δ cells demonstrated significant defects in spindle elongation. This result suggested that *ISC1* and *BUB1* genes play a crucial role in spindle elongation during mitosis. Previous studies had suggested a role for Bub3 in spindle elongation in the context of deletion of *CLB5* (35). The current results define a role for Bub1 in the spindle elongation in response to DNA damage. Importantly, the results now implicate sphingolipid metabolism in this process and specifically downstream of Bub1.

The results from this study specifically implicate bioactive lipids in a process that heretofore has not been appreciated to involve lipids or enzymes of lipid metabolism. Our previous results showed that *ISC1* activity was required for the HU response, and they further "triangulated" the lipid mediator of the action of *ISC1* in response to HU specifically to $C_{18:1}$ phytoceramide (24), one of at least 30 distinct ceramides present in yeast, thus indicating the operation of a very specific (and probably localized) sphingolipid pathway. The current results demonstrate that the $C_{18:1}$ fatty acid oleate, which is incorporated into $C_{18:1}$ ceramides (24), corrected the defect of growth on HU of the SLSP deletion mutants. These results provide further evidence of a role for sphingolipid metabolism downstream of the spindle checkpoint, demonstrating the essential role of one specific bioactive sphingolipid in the HU response involving Bub1, Mad1, Bim1, and Kar3.

A major mechanistic question to arise from these results concerns identification of downstream targets of *ISC1* and its lipid mediator $C_{18:1}$ phytoceramide. Our results clearly implicate both the Swe1 kinase and the Cdc55-containing protein phosphatase (of the PP2A family). Deletion of *SWE1* in *bub1*Δ, *mad1*Δ, and *bim1*Δ cells protected these mutants from HU toxicity, in a manner similar to protection seen in *isc1*Δ cells. Curiously, deletion of *SWE1* had no protective effect in *kar3*Δ cells. However, deletion of *SWE1* protected all mutants from the toxicity associated with benomyl.

Overexpression of *CDC55* rescued growth of *isc1*Δ, *bub1*Δ, *mad1*Δ, *bim1*Δ, and *kar3*Δ

cells. At this time, we cannot explain why *SWE1* deletion failed to protect *kar3*Δ cells from HU, but the results suggest that the *Kar3* gene has additional roles outside this pathway.

The emerging role of *CDC55* significantly builds on prior results with ceramide and protein phosphatases. A permeable form of ceramide, C2-ceramide, induced cell growth arrest in yeast cells, which were shown to exhibit a ceramide-activated phosphatase (36). Studies by Nickels and Broach identified the relevant phosphatase as the one involving the Sit4 catalytic subunit and the Cdc55 regulatory subunit (26). Interestingly, other studies have implicated *PP2A-CDC55* in spindle checkpoint adaptation (37, 38) and in the regulation of mitotic exit (39). In those studies, *PP2A-CDC55* is described as a negative regulator of anaphase onset, by preventing Net1 phosphorylation and Cdc14 activation and thus APC-cdc20 activation. Thus, taken together, the results from this study demonstrate the involvement of a phosphatase downstream of *ISC1* and $C_{18:1}$ phytoceramide leading to the execution component of the spindle checkpoint (Fig. 8).

Interestingly, *SWE1* has been shown to be essential in anaphase onset (40). During spindle checkpoint operation, anaphase onset is regulated by phosphorylation of cyclin-dependent kinase Cdc28. This kinase controls the metaphase anaphase transition, and mutations affecting Cdc28 or the two mitotic cyclins Clb1 and Clb2 delay anaphase initiation (41, 42). Swe1 is the kinase that phosphorylates Cdc28 and controls its activity and thus metaphase anaphase transition (40). More recently, Swe1 was shown to promote the G_0-S transition in a lipid-dependent manner; furthermore, Swe1 was found to be a level sensor and activator of sphingolipids (43, 44).

These results, revealing an intimate connection between *CDC55* and *SWE1*, suggest that Cdc55 can act in different possibilities that are not necessarily mutually exclusive (Fig. 8): (i) by regulating the levels of Swe1, thus influencing the phosphorylation of the downstream target Cdc28; (ii) by acting directly on Cdc28 and dephosphorylating the kinase to permit the metaphase-to-anaphase transition in the presence of benomyl or prolonged HU treatment; and/or (iii) by modulating the phosphorylation of Net1 and other possible substrates. Indeed, the phosphoproteomics of WT, *isc1*Δ, and *cdc55*Δ strains identified important additional substrates. Starting with 1184 HU-induced dephosphorylations, 264 proteins were identified as such in *isc1*Δ and *cdc55*Δ strains. Out of the 190 proteins dephosphorylated in an Isc1/Cdc55-dependent manner, 16 are involved in spindle assembly and chromatid separation. Within the 16 proteins, substrates of Cdc55 were identified: Orc2, Kin4, Sli15, Dam1, and She1, which connect the Isc1/phytoceramide/Cdc55 pathway to specific downstream cell processes (Fig. 8). The Kin4 protein is inactivated by dephosphorylation by Cdc55; this leads to Cdc14 activation through the mitotic exit network. On the other hand, Dam1, which was identified in this study as a new target of Cdc55, interacts with She1 to regulate the SAC. Indeed, the Dam1/DASH complex forms a ring around the attached microtubule and acts as a barrier between two proteins: Mps1 and its substrate, Spc105. This mechanical separation prevents interactions between Mps1 and Spc105 and thus inhibits the SAC signaling pathway (45).

We should note that in our hands, overexpression of the *MIH1* phosphatase, which is known to be involved in the G_2/M transition, did not protect cells from HU toxicity (data not shown), suggesting that the phosphatase that regulates anaphase onset, especially in the context of activation of Isc1, involves Cdc55 but not Mih1.

Interestingly, preliminary data showed that HU selectively induces an increase in the levels of the Isc1 protein in the nuclear fraction, thus placing all the components of this novel pathway (Bub1 and the SPLS proteins, Cdc55 and Swe1) in the nucleus (data not shown). These findings raise a number of intriguing questions on the localization and physical organization of lipids in the nucleus; however, an increasing body of literature points to the presence of specific bioactive lipids in the nucleus (46–49). Moreover, studies with mammals have also detected neutral sphingomyelinase (the mammalian counterpart of *ISC1*) (50–54) and sphingomyelin in the nucleus (55).

Taken together, the results from this study suggest that the lipid product of Isc1,

TABLE 3 Strains used in this study

Strain	Genotype	Origin
BY4741-WT	*MAT***a** *his3Δ1 leu2Δ0 met15Δ0 ura3Δ0*	Invitrogen deletion library
*isc1*Δ mutant	*MAT***a** *his3Δ1 leu2Δ0 met15Δ0 ura3Δ0 isc1::KanMX*	Invitrogen deletion library
*cdc55*Δ mutant	*MAT***a** *his3Δ1 leu2Δ0 met15Δ0 ura3Δ0 cdc55::KanMX*	Invitrogen deletion library
*bub1*Δ mutant	*MAT***a** *his3Δ1 leu2Δ0 met15Δ0 ura3Δ0 bub1::KanMX*	Invitrogen deletion library
*mad1*Δ mutant	*MAT***a** *his3Δ1 leu2Δ0 met15Δ0 ura3Δ0 mad1::KanMX*	Invitrogen deletion library
*bim1*Δ mutant	*MAT***a** *his3Δ1 leu2Δ0 met15Δ0 ura3Δ0 bim1::KanMX*	Invitrogen deletion library
*kar3*Δ mutant	*MAT***a** *his3Δ1 leu2Δ0 met15Δ0 ura3Δ0 kar3::KanMX*	Invitrogen deletion library
*swe1*Δ mutant	*MAT***a** *his3Δ1 leu2Δ0 met15Δ0 ura3Δ0 swe1::KanMX*	Invitrogen deletion library
*csm3*Δ mutant	*MAT***a** *his3Δ1 leu2Δ0 met15Δ0 ura3Δ0 csm3::KanMX*	Invitrogen deletion library
*ctf4*Δ mutant	*MAT***a** *his3Δ1 leu2Δ0 met15Δ0 ura3Δ0 ctf4::KanMX*	Invitrogen deletion library
*yke2*Δ mutant	*MAT***a** *his3Δ1 leu2Δ0 met15Δ0 ura3Δ0 yk2::KanMX*	Invitrogen deletion library
*dcc1*Δ mutant	*MAT***a** *his3Δ1 leu2Δ0 met15Δ0 ura3Δ0 dcc1::KanMX*	Invitrogen deletion library
*isc1*Δ *bub1*Δ mutant	*MAT***a** *his3Δ1 leu2Δ0 met15Δ0 ura3Δ0 bub1::KanMX isc1::HIS3*	Our laboratory collection
*isc1*Δ *mad1*Δ mutant	*MAT***a** *his3Δ1 leu2Δ0 met15Δ0 ura3Δ0 mad1::KanMX isc1::HIS3*	Our laboratory collection
*isc1*Δ *bim1*Δ mutant	*MAT***a** *his3Δ1 leu2Δ0 met15Δ0 ura3Δ0 bim1::KanMX isc1::HIS3*	Our laboratory collection
*isc1*Δ *kar3*Δ mutant	*MAT***a** *his3Δ1 leu2Δ0 met15Δ0 ura3Δ0 kar3::KanMX isc1::HIS3*	Our laboratory collection
*isc1*Δ *swe1*Δ mutant	*MAT***a** *his3Δ1 leu2Δ0 met15Δ0 ura3Δ0 isc1::KanMX swe1::LEU2*	Our laboratory collection
*bub1*Δ *swe1*Δ mutant	*MAT***a** *his3Δ1 leu2Δ0 met15Δ0 ura3Δ0 bub1::KanMX swe1::LEU2*	Our laboratory collection
*mad1*Δ *swe*Δ mutant	*MAT***a** *his3Δ1 leu2Δ0 met15Δ0 ura3Δ0 mad1::KanMX swe1::LEU2*	Our laboratory collection
*bim1*Δ *swe*Δ mutant	*MAT***a** *his3Δ1 leu2Δ0 met15Δ0 ura3Δ0 bim1::KanMX swe1::LEU2*	Our laboratory collection
*kar3*Δ *swe1*Δ mutant	*MAT***a** *his3Δ1 leu2Δ0 met15Δ0 ura3Δ0 kar3::KanMX swe1::LEU2*	Our laboratory collection
K6745	*MAT***a** *ade2-1 his3-11,15 Trp1-1 can1-100 GAL psi*$^{+}$ *leu2::LEU2 tetrGFP ura3::URA3 3x112 teto*	Nancy Hollingsworth's Laboratory
K6745 Δ	*MAT***a** *ade2-1 his3-11,15 Trp1-1 can1-100 GAL psi*$^{+}$ *leu2::LEU2 tetrGFP ura3::URA3 3x112 teto isc1::KanMX*	Our laboratory collection
BY4742-WT	*MATα his3Δ1 leu2Δ0 lys2Δ0 ura3Δ0*	Invitrogen deletion library
*isc1*Δ mutant	*MATα his3Δ1 leu2Δ0 lys2Δ0 ura3Δ0 isc1::KanMX*	Invitrogen deletion library
*cdc55*Δ mutant	*MATα his3Δ1 leu2Δ0 lys2Δ0 ura3Δ0 cdc55::KanMX*	Invitrogen deletion library
sli15 mutant	*MATα his3Δ1 leu2Δ0 lys2Δ0 ura3Δ0 sli15::KanMX*	Invitrogen deletion library
she1 mutantΔ	*MATα his3Δ1 leu2Δ0 lys2Δ0 ura3Δ0 she1::KanMX*	Invitrogen deletion library
Jk93dα-WT	*MATα leu2-3,112 ura3-52 trp1 his4 rme1*	Our laboratory collection
Jk9-3dα-*isc1*Δ	*MATα leu2-3,112 ura3-52 trp1 his4 rme1 isc1::KanMX*	Our laboratory collection
Jk9-3dα-*cdc55*Δ	*MATα leu2-3,112 ura3-52 trp1 his4 rme1 cdc55::KanMX*	Our laboratory collection

$C_{18:1}$ phytoceramide, functions as an intermediate molecule between the upstream SLPS genes, which constitute core components of G_2/M and spindle checkpoints, and the signal transmission downstream involving Swe1 and Cdc55 (Fig. 8). According to this hypothesis, when cells are treated with HU, a latent spindle checkpoint is activated. However, WT cells resume cycling by reentering into mitosis starting from spindle elongation and anaphase onset, resolving the spindle checkpoint blockage. To achieve the goal of resolving or overcoming the spindle checkpoint blockage, SLPS genes, in response to HU-induced damage, act on Isc1, increasing its activity to produce the signaling molecule $C_{18:1}$ phytoceramide. This molecule serves as an activator of Cdc55 and then Swe1 downstream, leading Cdc28, Kin4, Dam1, She1, and APC to permit the onset of anaphase. This study implicates another set of proteins, Siz1, Gac1, Ulp2, Top2, Sth1, Gip4, Spc29, Src1, and Fin1, as substrates of Cdc55. In conclusion, the results provide a very unexpected role for a nuclear pathway of sphingolipid metabolism mediated by Isc1 in the regulation of the spindle checkpoint, with Isc1 being necessary for signal transmission from Bub1, Mad1, and Bim1 to downstream targets Cdc55, Swe1 and Cdc28, Net1, Kin4, Dam1, and She1. The use of budding yeast as a model system with a combination of bioinformatic, biochemical, molecular, and phosphoproteomics approaches has provided unexpected and important biological insights that can be used as a valuable map to investigate the involvement of bioactive sphingolipids in eukaryotic cells.

MATERIALS AND METHODS

Strains used in this study are listed in Table 3.

Media. Standard yeast media—yeast extract, peptone, dextrose, and adenine (YPDA) medium, synthetic complete (SC) medium, and SD dropout medium lacking uracil (URA^{-})—were used in this study. Minimal SD base with galactose and raffinose URA^{-} dropout medium was used to overexpress

genes under the control of the GAL promoter, purchased from Clontech (no. 630420). HU was purchased from U.S. Biological and was employed at 7.5 mg/ml and 10 mg/ml in liquid and solid SC and YPDA media, respectively. Benomyl was purchased from U.S. Biological and used at 15 μg/ml and 24 μg/ml and in SC and YPDA media, respectively. Oleate was purchased from Sigma and used in solid agar medium at 0.003%.

Plasmids. YEp24 is a URA3 2μm autonomously replicating sequence (ARS) with multiple cloning sites. For YEp24 plus *CDC55*, the *CDC55* open reading frame was cloned into the YEp24 vector; for YEp24 plus *ISC1*, the *ISC1* open reading frame was cloned into the YEp24 vector); and for YEp24 plus *BUB1*, the *BUB1* open reading frame was cloned into the YEp24 vector. The PCR product was cloned using a PCR 2.1-TOPO vector from Invitrogen (catalog no. K4560-40; TOP10 competent bacterial cells purchased from Invitrogen were transformed with the made plasmid. Bacterial colonies grown on plates containing 50 μg/ml of carbenicillin were screened for positive clones containing the *CDC55* or the *BUB1* insert by digesting plasmid recovered by a standard Qiagen miniprep using BamHI and XhoI restriction enzymes. The positive clones were extracted from the gel and cloned into YEP24 vector. pYES2, a vector containing a galactose-inducible promoter, was purchased from Invitrogen. The *ISC1* open reading frame was cloned into pYES2 (pYES2 + *ISC1* [56]).

Spot test assays. Spot test assays were described previously (15). Briefly, cells were grown to stationary phase overnight, diluted to an optical density at 600 nm (OD_{600}) of 0.1, and then grown to an OD_{600} of 0.8. The cultures were diluted to an OD_{600} of 0.3 for the first spot on the left in all figures with spot tests. A series of 1:10 dilutions were spotted on YPD plates containing 10 mg/ml of HU or on SC plates containing 7.5 mg/ml of HU. YPD plates were incubated at 30°C for 3 days; SC or URA^- plates were incubated at 30°C for 4 to 5 days.

Protein preparation and Western blotting. Western blotting was performed as described previously (15). An anti-Myc tag was used to detect Swe1-Myc; anti-Swe1 from Santa Cruz Biotechnology (catalogue no. sc7171) was also used.

Antibody against Flag tag was used to detect ISC1-Flag. Antibody against PSTAIRE (PSTAIRE domain of Cdc2 p34; Santa Cruz Biotechnology [catalogue no. sc-53]) was used as a loading control.

Enzymatic activity assays. The assay for Isc1 activity was conducted as described previously (12). Briefly, sphingomyelin labeled with ^{14}C on the choline moiety was used as a substrate, and the hydrolysis of choline-*methyl*-[^{14}C]sphingomyelin was determined by liquid scintillation counting.

Lipid extraction and analysis. Lipid extraction and analysis have been described in detail previously (24).

Lipid analyses by HPLC-MS/MS. Levels of dihydroceramide, dihydroceramide, phytosphingosine, phytosphingosine 1-phosphate, dihydrosphingosine, and dihydrosphingosine 1-phosphate were measured by high-performance liquid chromatography–tandem mass spectrometry (LC-MS/MS) as previously described (57). Analytical results of lipids were expressed as lipid level/total cell number.

Lipid determination. Cells were grown overnight and then resuspended in the morning to an A_{600} of 0.15 in 50 ml of medium. Cells were grown to reach an A_{600} of 0.7 and then were treated with either HU or a vehicle. Cells were harvested after 3 and 20 h of treatment with HU. A_{600} was measured; all the cultures were diluted to an A_{600} of 0.7. Cells were then centrifuged at 3,000 $\times$ *g*, and the pellets were resuspended in 1 ml of a lipid extraction solvent containing isopropanol (50%), diethyl ether (10%), pyridine (2%), ammonia (25%), and water (15%). Acid-washed glass beads of 425 to 600 μm were added to a 200-μl volume. Tubes were placed on a Destroyer vortex for 5 repeats of a 3-min-on, 1-min-off regimen. The extracts were then transferred into 15-ml tubes, and the Eppendorf tubes used for lysis were washed with an additional 1 ml of extraction solvent and combined with the samples. The tubes containing approximately 2 ml of solvent, cells, and glass beads were used for lipid analysis (performed at the Lipidomic Core at the Medical University of South Carolina).

Microscopy. Briefly, cells (5×10^6 and 5×10^7) were harvested from logarithmic growth and resuspended in 5 ml of buffer. Then 0.5 ml of 37% formaldehyde was added, and cells were kept for at least 4 h at 4°C (for details, see reference 58). Slides were stored at −20°C and the cells were examined on a Nikon high-resolution microscope (simultaneous imaging) at the Stony Brook University Microscopy core.

Rebudding and sister chromatid separation assays. Wild-type cells treated with nocodazole activate the spindle assembly checkpoint and arrest as large budded cells in mitosis. However, checkpoint mutants continue through the cell cycle and pass through the subsequent G_1, generating a new bud. Overnight cultures in YPD medium were diluted 1:25. When cells reached an OD of ~0.3, they were treated with hydroxyurea for 4 h, washed twice, and then released into medium containing nocodazole (15 μg/ml). At each desired time point, cells were fixed in 4% paraformaldehyde at room temperature for 15 min, washed, and resuspended in a small volume of KPO_4-sorbitol solution. Cells were vortexed vigorously and examined by bright-field microscopy and categorized into G_1 (unbudded), dumbbell (large budded), and rebudded cells (more than one bud) as described before (38).

Strain K6745, originally from Koshland Lab at University of California (UC), Berkley, was a gift from Hollingsworth's Lab at Stony Brook University. Sister chromatid separation was monitored by using strain K6745 containing a Tet-GFP fusion and a tandem repeats of the *tet* operator inserted into the chromosome. Cells were treated as described for the rebudding assay, then fixed with paraformaldehyde for 10 min, washed, and resuspended in a small volume of KPO_4-sorbitol solution. Cells were analyzed using a Zeiss fluorescent microscope for the existence of one or two dots, corresponding to paired or separated sister chromatids, respectively. At least 200 cells were counted for each data point.

Data analysis. The genetic interaction data set was downloaded from the BioGRID database (http://thebiogrid.org), from which the yeast gene pairs that are either labeled as "synthetic lethality" or

"synthetic growth defect" were extracted. We used these interaction pairs to first identify the partners of the *ISC1* genes. These genes' genetic interaction partners were then extracted. A bipartite subgraph containing *ISC1* was identified from these genes. The number of genetic interaction partners shared by *ISC1* and each of the other members of the group in the bipartite graph was calculated. These genes were then mapped to the KEGG pathways to obtain the insight of their functions.

iTRAQ phosphoproteomics sample preparation. Jk9-3dα/vector, Jk9-3dα-*isc1*Δ/vector, Jk9-3dα-*cdc55*Δ/vector, and Jk9-3dα-*isc1*Δ/pYEP24-Cdc55 were cultured in yeast synthetic medium (SD-Ura) to logarithmic phase. Each culture was divided into two equal samples. Cultures were grown for another 3 h with one sample in the presence of 10 mg/ml of hydroxyurea, while the other was left untreated. A total of ~25 OD units of cells (1 OD unit $\approx 2 \times 10^7$ to 4×10^7 yeast cells) were collected from each sample by centrifugation at 3,000 rpm for 5 min. The cell pellets were frozen in liquid nitrogen immediately before being sent on dry ice to the phosphoproteomic facility.

iTRAQ labeling procedure. Samples were normalized to 160 μg of protein for each sample and were processed utilizing the standard ABSciex iTRAQ protocol (https://sciex.com/Documents/Downloads/Literature/mass-spectrometry-4375249C.pdf) utilizing all reagents included in the ABSciex 8-plex kit. The recommended 80 μg of peptide per sample was doubled to 160 μg to account for the low abundance of phosphopeptides. Therefore, two 8-Plex kits were utilized, with each sample requiring double the label. The nonmodified peptides and the phosphopeptides were all derived from the same iTRAQ samples. Prior to MS analysis, the iTRAQ-labeled peptides were separated into two pools of peptides. One of them were fractionated by hydrophilic interaction liquid chromatography (HILIC) and analyzed by MS (nonmodified), and the other pools were enriched for phosphopeptides by a TiO_2-SIMAC-HILIC (where SIMAC is sequential elution from immobilized metal affinity chromatography) procedure (https://www.ncbi.nlm.nih.gov/pubmed/22906719).

Capillary LC-mass spectrometry. An Orbitrap Velos Pro mass spectrometer (Thermo Scientific) equipped with a nano-ion spray source was coupled to an EASY-nLC system (Thermo Scientific). The nanoflow LC system was configured with a 180-μm (inside diameter) fused silica capillary trap column containing 3 cm of Aqua 5-μm C_{18} material (Phenomenex), and a self-pack PicoFrit 100-μm analytical column with an 8-μm emitter (New Objective, Woburn, MA) packed to 15 cm with Aqua 3-μm C_{18} material (Phenomenex). Mobile phase A consisted of 2% acetonitrile-0.1% formic acid, and mobile phase B consisted of 90% acetonitrile-0.1% formic acid. An aliquot of 3 μl of each sample dissolved in mobile phase A was injected through the autosampler onto the trap column. Peptides were then separated using the following linear gradient steps at a flow rate of 400 nl/min: 5% mobile phase B for 1 min, 5% mobile phase B to 35% mobile phase B over 70 min, 35% B to 75% mobile phase B over 15 min, holding at 75% mobile phase B for 8 min, 75% mobile phase B to 8% mobile phase B over 1 min, and holding at 8% mobile phase B for the final 5 min.

Eluted peptides were directly electrosprayed into the Orbitrap Velos Pro mass spectrometer with the application of a distal 2.3-kV spray voltage and a capillary temperature of 275°C. Each full-scan mass spectrum (resolution = 60,000; 380 to 1,700 *m/z*) was followed by MS/MS spectra for the top 12 masses. High-energy collisional dissociation (HCD) was used with the normalized collision energy set to 35 for fragmentation, the isolation width set to 1.2, and an activation time of 0.1. A duration of 30 s was set for the dynamic exclusion with an exclusion list size of 500, repeat count of 1, and exclusion mass width of 10 ppm. We used monoisotopic precursor selection for charge states 2+ and greater, and all data were acquired in profile mode.

Database Searching-Peaklist files were generated by Mascot Distiller (Matrix Science). Protein identification and quantification were carried using Mascot 2.2 (59) against the Uniprot Human sequence database (89,706 sequences; 35,609,686 residues). Secondary searches were performed utilizing Thermo Proteome Discoverer. Methylthiolation of cysteine and N-terminal and lysine iTRAQ modifications were set as fixed modifications, methionine oxidation and deamidation (NQ) as variable. Trypsin was used as a cleavage enzyme, with one missed cleavage allowed. Mass tolerance was set at 30 ppm for intact peptide mass and 0.3 Da for fragment ions. Search results were rescored to give a final 1% false-discovery rate (FDR) using a randomized version of the same Uniprot human database. Protein-level iTRAQ ratios were calculated as intensity weighted, using only peptides with expectation values of <0.05. Global ratio normalization (summed) was applied across all iTRAQ channels. Phosphopeptides were normalized to their corresponding unmodified proteins when possible. Protein enrichment was then calculated by dividing sample protein ratios by the corresponding control sample channel.

Phosphoproteomics data analysis. Samples of wild-type Jk9-3dα, Jk9-3dα-*isc1*Δ mutant, Jk9-3dα-*cdc55*Δ mutant, and Jk9-3dα-*isc1*Δ mutant cells overexpressing Cdc55 (Cdc55-OE) were treated with HU or left untreated. In total, eight conditions were analyzed by iTRAQ, resulting in a total of 20,758 phosphopeptide hits. Phosphopeptide abundances were normalized for protein concentration before further analysis and sorted as follows: WT plus HU phosphopeptide abundances were normalized to the WT, and the ratios of (WT plus HU)/WT were calculated and sorted using Excel. A total of 1,184 peptides which displayed a ratio R of <0.6 (a decrease in phosphorylation levels as a result of HU treatment) were selected for further analysis. Starting with the 1,184 selected peptides, Isc1 plus HU phosphopeptide abundances were normalized to Isc1 and sorted using Excel. Isc1 plus HU phosphopeptides with $0.7 < R < 1.3$ were selected and considered Isc1-dependent dephosphorylations (545 phosphopeptides). Like Isc1 selection, starting with the 1,184 peptides, Cdc55 plus HU phosphopeptide abundances were normalized to Cdc55 and sorted using Excel. Cdc55 plus HU phosphopeptides with $0.7 < R < 1.3$ were selected and considered Cdc55-dependent dephosphorylations (656 phosphopeptides). Starting with the Isc1-dependent dephosphorylation hits we obtained as described above (545 phosphopeptides), Cdc55-OE plus HU phosphopeptide abundances were normalized to Cdc55-OE and sorted using Excel.

Cdc55-OE plus HU phosphopeptides with $0 < R < 0.75$ were selected and considered Isc1-dependent dephosphorylations reversed by Cdc55 overexpression (190 proteins).

ACKNOWLEDGMENTS

This work was supported by NIH grant GM118128 to Y.A.H. and grants P20 RR017696, P20 RR017677, CPRIT RP170668, and LM 010680 to W.J.Z.

Microscopy was performed at the Central Microscopy Imaging Center (CMIC) at Stony Brook University. We thank Guowei Tian for his help and support in microscopy and Nancy Hollingsworth at Stony Brook University, Department of Biochemistry and Cell Biology, for providing us with the K6745 strain. We also thank the lipidomic core at Stony Brook University for the lipid analysis. We thank the KEGG/GenomeNet team for granting copyright permission to publish Fig. 1B.

Author contributions are as follows: conceptualization, N.M., B.H.H., W.J.Z., and Y.A.H.; methodology and investigation, N.M., B.H.H., A.A.S., E.J., B.S., and G.C.; genetic interaction analysis, W.J.Z.; phosphoproteomics analysis, N.M., B.H.H., J.R., A.A.S., J.S., S.V.R., M.R.L., and N.J.F.; writing of original draft, N.M. and Y.A.H.; writing, review, and editing, N.M., B.H.H., J.R., B.K.M., W.J.Z., N.J.F., L.M.O., and Y.A.H.; and funding acquisition, Y.A.H.

We declare no competing interests.

REFERENCES

1. Hartwell LH, Kastan MB. 1994. Cell cycle control and cancer. Science 266:1821–1828. https://doi.org/10.1126/science.7997877.
2. Sansregret L, Swanton C. 2017. The role of aneuploidy in cancer evolution. Cold Spring Harb Perspect Med 7:a028373. https://doi.org/10.1101/cshperspect.a028373.
3. Rudner AD, Murray AW. 1996. The spindle assembly checkpoint. Curr Opin Cell Biol 8:773–780. https://doi.org/10.1016/s0955-0674(96)80077-9.
4. Pan J, Chen RH. 2004. Spindle checkpoint regulates Cdc20p stability in Saccharomyces cerevisiae. Genes Dev 18:1439–1451. https://doi.org/10.1101/gad.1184204.
5. Hannun YA, Obeid LM. 2008. Principles of bioactive lipid signalling: lessons from sphingolipids. Nat Rev Mol Cell Biol 9:139–150. https://doi.org/10.1038/nrm2329.
6. Chalfant CE, Spiegel S. 2005. Sphingosine 1-phosphate and ceramide 1-phosphate: expanding roles in cell signaling. J Cell Sci 118:4605–4612. https://doi.org/10.1242/jcs.02637.
7. Hannun YA, Obeid LM. 2018. Sphingolipids and their metabolism in physiology and disease. Nat Rev Mol Cell Biol 19:175–191. https://doi.org/10.1038/nrm.2017.107.
8. Dickson RC. 1998. Sphingolipid functions in Saccharomyces cerevisiae: comparison to mammals. Annu Rev Biochem 67:27–48. https://doi.org/10.1146/annurev.biochem.67.1.27.
9. Epstein S, Riezman H. 2013. Sphingolipid signaling in yeast: potential implications for understanding disease. Front Biosci (Elite Ed) 5:97–108. https://doi.org/10.2741/e599.
10. Montefusco DJ, Matmati N, Hannun YA. 2014. The yeast sphingolipid signaling landscape. Chem Phys Lipids 177:26–40. https://doi.org/10.1016/j.chemphyslip.2013.10.006.
11. Malagarie-Cazenave S, Andrieu-Abadie N, Ségui B, Gouazé V, Tardy C, Cuvillier O, Levade T. 2002. Sphingolipid signalling: molecular basis and role in TNF-alpha-induced cell death. Expert Rev Mol Med 4:1–15. https://doi.org/10.1017/S146239940200546X.
12. Sawai H, Okamoto Y, Luberto C, Mao C, Bielawska A, Domae N, Hannun YA. 2000. Identification of ISC1 (YER019w) as inositol phosphosphingolipid phospholipase C in Saccharomyces cerevisiae. J Biol Chem 275:39793–39798. https://doi.org/10.1074/jbc.M007721200.
13. Almeida T, Marques M, Mojzita D, Amorim MA, Silva RD, Almeida B, Rodrigues P, Ludovico P, Hohmann S, Moradas-Ferreira P, Côrte-Real M, Costa V. 2008. Isc1p plays a key role in hydrogen peroxide resistance and chronological lifespan through modulation of iron levels and apoptosis. Mol Biol Cell 19:865–876. https://doi.org/10.1091/mbc.e07-06-0604.
14. Hannun YA, Obeid LM. 2011. Many ceramides. J Biol Chem 286:27855–27862. https://doi.org/10.1074/jbc.R111.254359.
15. Matmati N, Kitagaki H, Montefusco D, Mohanty BK, Hannun YA. 2009. Hydroxyurea sensitivity reveals a role for ISC1 in the regulation of G2/M. J Biol Chem 284:8241–8246. https://doi.org/10.1074/jbc.M900004200.
16. Zhu L, Zheng WJ. 2018. Informatics, data science, and artificial intelligence. JAMA 320:1103–1104. https://doi.org/10.1001/jama.2018.8211.
17. Boone C, Bussey H, Andrews BJ. 2007. Exploring genetic interactions and networks with yeast. Nat Rev Genet 8:437–449. https://doi.org/10.1038/nrg2085.
18. Kelley R, Ideker T. 2005. Systematic interpretation of genetic interactions using protein networks. Nat Biotechnol 23:561–566. https://doi.org/10.1038/nbt1096.
19. Ulitsky I, Shamir R. 2007. Pathway redundancy and protein essentiality revealed in the Saccharomyces cerevisiae interaction networks. Mol Syst Biol 3:104. https://doi.org/10.1038/msb4100144.
20. Ye P, Peyser BD, Pan X, Boeke JD, Spencer FA, Bader JS. 2005. Gene function prediction from congruent synthetic lethal interactions in yeast. Mol Syst Biol 1:2005.0026. https://doi.org/10.1038/msb4100034.
21. Ma X, Tarone AM, Li W. 2008. Mapping genetically compensatory pathways from synthetic lethal interactions in yeast. PLoS One 3:e1922. https://doi.org/10.1371/journal.pone.0001922.
22. Mayer ML, Pot I, Chang M, Xu H, Aneliunas V, Kwok T, Newitt R, Aebersold R, Boone C, Brown GW, Hieter P. 2004. Identification of protein complexes required for efficient sister chromatid cohesion. Mol Biol Cell 15:1736–1745. https://doi.org/10.1091/mbc.e03-08-0619.
23. Xu H, Boone C, Brown GW. 2007. Genetic dissection of parallel sister-chromatid cohesion pathways. Genetics 176:1417–1429. https://doi.org/10.1534/genetics.107.072876.
24. Matmati N, Metelli A, Tripathi K, Yan S, Mohanty BK, Hannun YA. 2013. Identification of C18:1-phytoceramide as the candidate lipid mediator for hydroxyurea resistance in yeast. J Biol Chem 288:17272–17284. https://doi.org/10.1074/jbc.M112.444802.
25. Straight AF, Murray AW. 1997. The spindle assembly checkpoint in budding yeast. Methods Enzymol 283:425–440. https://doi.org/10.1016/s0076-6879(97)83035-2.
26. Nickels JT, Broach JR. 1996. A ceramide-activated protein phosphatase mediates ceramide-induced G1 arrest of Saccharomyces cerevisiae. Genes Dev 10:382–394. https://doi.org/10.1101/gad.10.4.382.
27. Baro B, Játiva S, Calabria I, Vinaixa J, Bech-Serra J-J, de LaTorre C, Rodrigues J, Hernáez ML, Gil C, Barceló-Batllori S, Larsen MR, Queralt E. 2018. SILAC-based phosphoproteomics reveals new PP2A-Cdc55-regulated processes in budding yeast. Gigascience 7:giy047. https://doi.org/10.1093/gigascience/giy047.
28. Shimada K, Gasser SM. 2007. The origin recognition complex functions in sister-chromatid cohesion in Saccharomyces cerevisiae. Cell 128:85–99. https://doi.org/10.1016/j.cell.2006.11.045.
29. Carmena M, Wheelock M, Funabiki H, Earnshaw WC. 2012. The chromosomal passenger complex (CPC): from easy rider to the godfather of mitosis. Nat Rev Mol Cell Biol 13:789–803. https://doi.org/10.1038/nrm3474.
30. Martin-Lluesma S, Stucke VM, Nigg EA. 2002. Role of Hec1 in spindle

checkpoint signaling and kinetochore recruitment of Mad1/Mad2. Science 297:2267–2270. https://doi.org/10.1126/science.1075596.
31. Musacchio A, Salmon ED. 2007. The spindle-assembly checkpoint in space and time. Nat Rev Mol Cell Biol 8:379–393. https://doi.org/10.1038/nrm2163.
32. Mayer ML, Gygi SP, Aebersold R, Hieter P. 2001. Identification of RFC(Ctf18p, Ctf8p, Dcc1p): an alternative RFC complex required for sister chromatid cohesion in S. cerevisiae. Mol Cell 7:959–970. https://doi.org/10.1016/S1097-2765(01)00254-4.
33. Skibbens RV, Hieter P. 1998. Kinetochores and the checkpoint mechanism that monitors for defects in the chromosome segregation machinery. Annu Rev Genet 32:307–337. https://doi.org/10.1146/annurev.genet.32.1.307.
34. Nasmyth K. 2002. Segregating sister genomes: the molecular biology of chromosome separation. Science 297:559–565. https://doi.org/10.1126/science.1074757.
35. Ikui AE, Cross FR. 2009. Specific genetic interactions between spindle assembly checkpoint proteins and B-Type cyclins in Saccharomyces cerevisiae. Genetics 183:51–61. https://doi.org/10.1534/genetics.109.105148.
36. Fishbein JD, Dobrowsky RT, Bielawska A, Garrett S, Hannun YA. 1993. Ceramide-mediated growth inhibition and CAPP are conserved in Saccharomyces cerevisiae. J Biol Chem 268:9255–9261.
37. Vernieri C, Chiroli E, Francia V, Gross F, Ciliberto A. 2013. Adaptation to the spindle checkpoint is regulated by the interplay between Cdc28/Clbs and PP2ACdc55. J Cell Biol 202:765–778. https://doi.org/10.1083/jcb.201303033.
38. Rossio V, Michimoto T, Sasaki T, Ohbayashi I, Kikuchi Y, Yoshida S. 2013. Nuclear PP2A-Cdc55 prevents APC-Cdc20 activation during the spindle assembly checkpoint. J Cell Sci 126:4396–4405. https://doi.org/10.1242/jcs.127365.
39. Queralt E, Lehane C, Novak B, Uhlmann F. 2006. Downregulation of PP2A(Cdc55) phosphatase by separase initiates mitotic exit in budding yeast. Cell 125:719–732. https://doi.org/10.1016/j.cell.2006.03.038.
40. Lianga N, Williams EC, Kennedy EK, Dore C, Pilon S, Girard SL, Deneault JS, Rudner AD. 2013. A Wee1 checkpoint inhibits anaphase onset. J Cell Biol 201:843–862. https://doi.org/10.1083/jcb.201212038.
41. Rudner AD, Murray AW. 2000. Phosphorylation by Cdc28 activates the Cdc20-dependent activity of the anaphase-promoting complex. J Cell Biol 149:1377–1390. https://doi.org/10.1083/jcb.149.7.1377.
42. Rahal R, Amon A. 2008. Mitotic CDKs control the metaphase-anaphase transition and trigger spindle elongation. Genes Dev 22:1534–1548. https://doi.org/10.1101/gad.1638308.
43. Chauhan N, Visram M, Cristobal-Sarramian A, Sarkleti F, Kohlwein SD. 2015. Morphogenesis checkpoint kinase Swe1 is the executor of lipolysis-dependent cell-cycle progression. Proc Natl Acad Sci U S A 112:E1077–E1085. https://doi.org/10.1073/pnas.1423175112.
44. Chauhan N, Han G, Somashekarappa N, Gable K, Dunn T, Kohlwein SD. 2016. Regulation of sphingolipid biosynthesis by the morphogenesis checkpoint kinase Swe1. J Biol Chem 291:2524–2534. https://doi.org/10.1074/jbc.M115.693200.
45. Aravamudhan P, Goldfarb AA, Joglekar AP. 2015. The kinetochore encodes a mechanical switch to disrupt spindle assembly checkpoint signalling. Nat Cell Biol 17:868–879. https://doi.org/10.1038/ncb3179.
46. Ramazzotti G, Faenza I, Fiume R, Matteucci A, Piazzi M, Follo MY, Cocco L. 2011. The physiology and pathology of inositide signaling in the nucleus. J Cell Physiol 226:14–20. https://doi.org/10.1002/jcp.22334.
47. Cocco L, Martelli AM, Fiume R, Faenza I, Billi AM, Manzoli FA. 2006. Signal transduction within the nucleus: revisiting phosphoinositide inositide-specific phospholipase Cbeta1. Adv Enzyme Regul 46:2–11. https://doi.org/10.1016/j.advenzreg.2006.01.012.
48. Faenza I, Fiume R, Piazzi M, Colantoni A, Cocco L. 2013. Nuclear inositide specific phospholipase C signalling—interactions and activity. FEBS J 280:6311–6321. https://doi.org/10.1111/febs.12450.
49. Follo MY, Marmiroli S, Faenza I, Fiume R, Ramazzotti G, Martelli AM, Gobbi P, McCubrey JA, Finelli C, Manzoli FA, Cocco L. 2013. Nuclear phospholipase C beta1 signaling, epigenetics and treatments in MDS. Adv Biol Regul 53:2–7. https://doi.org/10.1016/j.jbior.2012.09.009.
50. Albi E, Cataldi S, Rossi G, Magni MV. 2003. A possible role of cholesterol-sphingomyelin/phosphatidylcholine in nuclear matrix during rat liver regeneration. J Hepatol 38:623–628. https://doi.org/10.1016/s0168-8278(03)00074-6.
51. Albi E, Lazzarini R, Magni MV. 2003. Reverse sphingomyelin-synthase in rat liver chromatin. FEBS Lett 549:152–156. https://doi.org/10.1016/s0014-5793(03)00810-x.
52. Albi E, Rossi G, Maraldi NM, Magni MV, Cataldi S, Solimando L, Zini N. 2003. Involvement of nuclear phosphatidylinositol-dependent phospholipases C in cell cycle progression during rat liver regeneration. J Cell Physiol 197:181–188. https://doi.org/10.1002/jcp.10292.
53. Alessenko A, Chatterjee S. 1995. Neutral sphingomyelinase: localization in rat liver nuclei and involvement in regeneration/proliferation. Mol Cell Biochem 143:169–174. https://doi.org/10.1007/bf01816950.
54. Romanenko EB, Alessenko AV, Vanyushin BF. 1995. Effect of sphingomyelin and antioxidants on the in vitro and in vivo DNA methylation. Biochem Mol Biol Int 35:87–94.
55. Sobol M, Krausová A, Yildirim S, Kalasová I, Fáberová V, Vrkoslav V, Philimonenko V, Marášek P, Pastorek L, Čapek M, Lubovská Z, Uličná L, Tsuji T, Lísa M, Cvačka J, Fujimoto T, Hozak P. 2018. Nuclear phosphatidylinositol 4,5-bisphosphate islets contribute to efficient RNA polymerase II-dependent transcription. J Cell Sci 131:jcs211094. https://doi.org/10.1242/jcs.211094.
56. Okamoto Y, Vaena de Avalos S, Hannun YA. 2003. Functional analysis of ISC1 by site-directed mutagenesis. Biochemistry 42:7855–7862. https://doi.org/10.1021/bi0341354.
57. Bielawski J, Pierce JS, Snider J, Rembiesa B, Szulc ZM, Bielawska A. 2010. Sphingolipid analysis by high performance liquid chromatography-tandem mass spectrometry (HPLC-MS/MS). Adv Exp Med Biol 688:46–59. https://doi.org/10.1007/978-1-4419-6741-1_3.
58. Kilmartin JV, Adams AE. 1984. Structural rearrangements of tubulin and actin during the cell cycle of the yeast Saccharomyces. J Cell Biol 98:922–933. https://doi.org/10.1083/jcb.98.3.922.
59. Perkins DN, Pappin DJ, Creasy DM, Cottrell JS. 1999. Probability-based protein identification by searching sequence databases using mass spectrometry data. Electrophoresis 20:3551–3567. https://doi.org/10.1002/(SICI)1522-2683(19991201)20:18<3551::AID-ELPS3551>3.0.CO;2-2.
60. Albuquerque CP, Smolka MB, Payne SH, Bafna V, Eng J, Zhou H. 2008. A multidimensional chromatography technology for in-depth phosphoproteome analysis. Mol Cell Proteomics 7:1389–1396. https://doi.org/10.1074/mcp.M700468-MCP200.
61. Harvey SL, Charlet A, Haas W, Gygi SP, Kellogg DR. 2005. Cdk1-dependent regulation of the mitotic inhibitor Wee1. Cell 122:407–420. https://doi.org/10.1016/j.cell.2005.05.029.
62. Breitkreutz A, Choi H, Sharom JR, Boucher L, Neduva V, Larsen B, Lin ZY, Breitkreutz BJ, Stark C, Liu G, Ahn J, Dewar-Darch D, Reguly T, Tang X, Almeida R, Qin ZS, Pawson T, Gingras AC, Nesvizhskii AI, Tyers M. 2010. A global protein kinase and phosphatase interaction network in yeast. Science 328:1043–1046. https://doi.org/10.1126/science.1176495.
63. Gnad F, de Godoy LM, Cox J, Neuhauser N, Ren S, Olsen JV, Mann M. 2009. High-accuracy identification and bioinformatic analysis of in vivo protein phosphorylation sites in yeast. Proteomics 9:4642–4652. https://doi.org/10.1002/pmic.200900144.
64. Soufi B, Kelstrup CD, Stoehr G, Fröhlich F, Walther TC, Olsen JV. 2009. Global analysis of the yeast osmotic stress response by quantitative proteomics. Mol Biosyst 5:1337–1346. https://doi.org/10.1039/b902256b.
65. Holt LJ, Tuch BB, Villén J, Johnson AD, Gygi SP, Morgan DO. 2009. Global analysis of Cdk1 substrate phosphorylation sites provides insights into evolution. Science 325:1682–1686. https://doi.org/10.1126/science.1172867.
66. Pereira G, Schiebel E. 2003. Separase regulates INCENP-Aurora B anaphase spindle function through Cdc14. Science 302:2120–2124. https://doi.org/10.1126/science.1091936.
67. Cheeseman IM, Anderson S, Jwa M, Green EM, Kang Js, Yates JR, III, Chan CS, Drubin DG, Barnes G. 2002. Phospho-regulation of kinetochore-microtubule attachments by the Aurora kinase Ipl1p. Cell 111:163–172. https://doi.org/10.1016/S0092-8674(02)00973-X.
68. Keating P, Rachidi N, Tanaka TU, Stark MJ. 2009. Ipl1-dependent phosphorylation of Dam1 is reduced by tension applied on kinetochores. J Cell Sci 122:4375–4382. https://doi.org/10.1242/jcs.055566.
69. Soulard A, Cremonesi A, Moes S, Schütz F, Jenö P, Hall MN. 2010. The rapamycin-sensitive phosphoproteome reveals that TOR controls protein kinase A toward some but not all substrates. Mol Biol Cell 21:3475–3486. https://doi.org/10.1091/mbc.E10-03-0182.
70. Caydasi AK, Kurtulmus B, Orrico MI, Hofmann A, Ibrahim B, Pereira G. 2010. Elm1 kinase activates the spindle position checkpoint kinase Kin4. J Cell Biol 190:975–989. https://doi.org/10.1083/jcb.201006151.